Eur. Phys. J. Plus (2017) **132**: 6
DOI 10.1140/epjp/i2017-11275-5

THE EUROPEAN PHYSICAL JOURNAL PLUS

Regular Article

Critical speed and free vibration analysis of spinning 3D single-walled carbon nanotubes resting on elastic foundations

Mohammad Mostafa Barooti, Hamed Safarpour, and Majid Ghadiri[a]

Faculty of Engineering, Department of Mechanics, Imam Khomeini International University, Postal code 3414916818, Qazvin, Iran

Received: 26 October 2016 / Revised: 24 November 2016
Published online: 12 January 2017 –

Abstract. In this article, the influences of critical speed on the free vibration behavior of spinning 3D single-walled carbon nanotubes (SWCNT) are investigated using modified couple stress theory (MCST). Moreover, the surrounding elastic medium of SWCNT has been considered as a model of Winkler, characterized by the spring. Taking into consideration the first-order shear deformation theory (FSDT), the rotating SWCNT is modeled and its equations of motion are derived using the Hamilton principle. The formulations include Coriolis, centrifugal and initial hoop tension effects due to rotation of the SWCNT. The accuracy of the presented model is validated by some cases in the literature. The novelty of this study is considering the effects of rotation and MCST, in addition to considering the various boundary conditions of SWCNT. The generalized differential quadrature method (GDQM) is used to discretize the model and to approximate the equation of motion. Then investigation has been made on critical speed and natural frequency of the rotating SWCNT due to the influence of initial hoop tension, material length scale parameter, constant of spring, frequency mode number, angular velocity, length-to-radius ratio, radius-to-thickness ratio and boundary conditions.

1 Introduction

Owing to the recent advancement in science and technology, SWCNT have attracted considerable attention. The surprising mechanical properties of SWCNT make them an appropriate choice to be used in chemistry, physics, and nano-engineering applications, as well as for practical use in electrical engineering, materials science and construction engineering. Therefore, it is vital to study the mechanical behavior of SWCNT, such as buckling and post-buckling [1], vibration [2], thermal vibration [3] and instability analysis [4]. As examples of some SWCNT applications, one can name drug delivery [5], micro-/nano-electromechanical systems (MEMS/NEMS) [6] and nanopipes containing a flowing fluid [7]. Rotating SWCNT have caught eyes, in recent years, owing to their promising future. These rotating nanostructures can also be used as MEMS gyroscope sensors [8] in the aerospace industry, military, automotive and consumer electronics markets, including advanced automotive safety systems, high-performance navigation and guidance systems, ride stabilization, roll-over detection and prevention, image stabilization in digital cameras and highly technological applications including nano-/micro-satellites, nano-/micro-robotics, and even implantable devices to cure internal disorders. Lately, Tu *et al.* [9] have suggested a rotating membrane filter made of a carbon nanotube for desalinating water, which proves this study precious. The experiments and researches show that the size effects play an important role in mechanical properties [10,11]. Thus, avoiding these effects may result in wrong designs and unacceptable answers. It should be mentioned that the size effect is not considered in the classical continuum theories, so this theory is not appropriate for micro and nano scales. One of the non-classical theories that consider the effects of size is the couple stress theory. Toupin, Koiter, and Mindlin [12–14] investigated the couple stress theory including higher-order rotation gradients, which is in fact the asymmetric part of the deformation gradient. According to this theory, it includes four material constants (two classical ones and two additional ones) for isotropic elastic materials. As an example of this theory, Asghari *et al.* [15] presented the size effects in Timoshenko beams based on the couple stress theory. It is difficult to determine whether the microstructure depends on length scale parameters. Therefore, we are looking for a continuum theory which involves only one additional material parameter of length scale. MCST is one of the best and most well-known continuum mechanics theories which include small-scale effects with reasonable accuracy in micro-scale devices.

[a] e-mail: ghadiri@eng.ikiu.ac.ir (corresponding author)

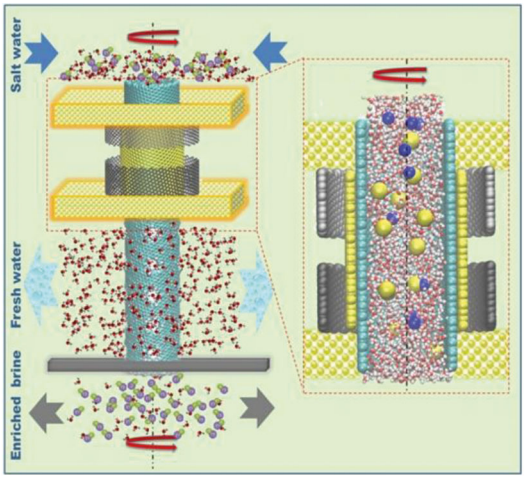

Fig. 1. An application of a rotating SWCNT [9].

Yang *et al.* [16] presented a modified couple stress theory, in which the couple stress tensor is symmetric and there is only one internal material length scale parameter involved, unlike the classical couple stress theory mentioned above. Many researchers have used this theory to examine the dynamic and static behavior of micro-beams and micro-plates [17–19]. It is noted that the non-local theory of Eringen is one of the best and most well-known continuum mechanics theories which includes small scale effects with sufficient accuracy in nano-/micro-scale devices, but the results show that modified couple stress theory which coincides with experimental results is better than Eringen's non-local elasticity and classical theories [20]. Therefore, in this study, the modified couple stress theory has been used. In the theories of classical shell, it is assumed that the stresses are constant within the thickness. Consequently, due to this assumption, the theories of classical shell cannot present precise results for thick and moderately thick shells. The first-order shear deformation theory (FSDT) was presented by Reissner [21] and Mindlin [22] to compensate classical theory for its defects. Researchers show that the dynamic behavior of carbon nanotube is substantially similar to those of cylindrical shell [23]. Consequently, for a better comprehension of nanotube rotational behavior, the rotational behavior of a cylinder should be studied first. The dynamic analysis of rotating cylindrical shell has been carried out since about one century ago. At first, Bryan [24] analyzed a rotating cylindrical shell, considering a rotating ring. He found the traveling mode phenomenon for the first time. Years later, Taranto and Lesson [25] studied the rotating shells, considering the Coriolis effect. Zohar and Aboudi [26] worked on a rotating finite thin cylinder. Simultaneously, Padovan [27] was doing research into natural frequencies of rotating prestressed cylinder using thin shell theory. He also utilized numerical and finite element method to predict asymmetric frequencies and buckling loads [28,29]. A decade later, Endo *et al.* [30] theoretically obtained flexural vibration of a thin cylindrical ring, and compared their findings with experiment. Two years later, Saito and Endo [31] modified their previous studies considering initial tension. All of the researches were undertaken into free vibration of rotating cylinders thus far, but Huang and Soedel [32] undertook research into free and forced vibration of a finite cylinder with simply supported boundaries. As a main result, they came to a major conclusion that rotation compels natural frequencies to bifurcate into two branches. Moreover, Huang and Hsu [33] studied the influence of a harmonic moving load on the resonant of a rotating cylindrical shell. It is worth mentioning that none of the previous works have considered the size effect and initial hoop tension on a rotating SWCNT using MCST. The novelty of this work is considering rotation, initial hoop tension and size effect in addition to considering various boundary conditions on SWCNT using MCST. Because of the high accuracy and efficiency of the generalized differential quadrature method (GDQM), it is utilized to solve the governing equation of the problem for each kinds of boundary condition. The governing equations and boundary conditions, which have been developed using the Hamilton principle, are solved with the aid of GDQM. The results show that initial hoop tension, material length scale parameter, constant of spring, angular velocity, length-to-radius ratio, radius-to-thickness ratio and boundary conditions play important roles on the natural frequency and critical angular velocity of a rotating SWCNT.

2 Size-dependent spinning SWCNT resting on elastic foundation equations

To have a better understanding of the importance and applications of the proposed model, fig. 1 demonstrates a rotating SWCNT which can turn salt water into fresh water [9]. In addition, fig. 2 shows a spinning SWCNT, where x, θ, and z denote the orthogonal curvilinear coordinates on the middle surface ($z = 0$). The thickness, length, and the middle surface radius of SWCNT are denoted by h, L, and R, respectively. Moreover, the surrounding elastic medium of SWCNT has been considered as a model of Winkler, characterized by the spring.

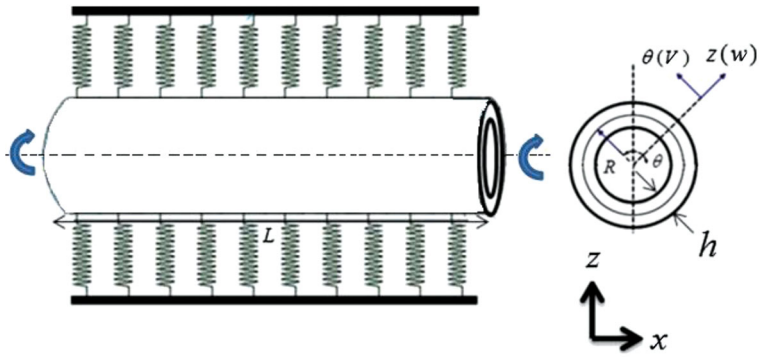

Fig. 2. The geometry of a spinning SWCNT resting on elastic foundation.

2.1 Modified couple stress theory

Yang *et al.* [16] presented modified couple stress theory for the first time. According to this theory, the strain energy expressed as a function of rotation tensor gradient and strain tensor, in addition, it includes one length scale parameter and two Lamé parameters. With regard to this theory, the strain energy is expressed as

$$U = \frac{1}{2}\iiint_V (\sigma_{ij}\varepsilon_{ij} + m^s_{ij}\chi^s_{ij})\mathrm{d}V. \tag{1}$$

In eq. (1), χ^s_{ij}, ε_{ij}, σ_{ij} and m_{ij}, respectively, represent the components of a symmetric rotation gradient tensor, strain tensor, stress tensor, and higher-order stress tensor, which are expressed as

$$\varepsilon_{ij} = \frac{1}{2}(u_{i,j} + u_{j,i}) \tag{2}$$

$$\chi^s_{ij} = \frac{1}{2}(\varphi_{i,j} + \varphi_{j,i}) \tag{3}$$

$$m^s_{ij} = 2l^2\mu(\hat{z})\chi^s_{ij}, \qquad \varphi_i = \frac{1}{2}\left[\mathrm{curl}(u)\right]_i, \tag{4}$$

where u_i and φ_i, respectively, represent the component of displacement vector, and extremely small rotation vector. In eq. (4), l is a parameter which denotes an additional independent material length scale parameter, which is related to symmetric rotation gradients. Note that the length scale parameter is assumed as constant in SWCNT. In addition, the stress-strain relation can be expressed as follows:

$$\begin{Bmatrix} \sigma_{xx} \\ \sigma_{\theta\theta} \\ \sigma_{x\theta} \\ \sigma_{\theta z} \\ \sigma_{xz} \end{Bmatrix} = \begin{bmatrix} C_{11} & C_{12} & 0 & 0 & 0 \\ C_{12} & C_{22} & 0 & 0 & 0 \\ 0 & 0 & C_{66} & 0 & 0 \\ 0 & 0 & 0 & C_{44} & 0 \\ 0 & 0 & 0 & 0 & C_{55} \end{bmatrix} \begin{Bmatrix} \varepsilon_{xx} \\ \varepsilon_{\theta\theta} \\ 2\varepsilon_{x\theta} \\ 2\varepsilon_{\theta z} \\ 2\varepsilon_{xz} \end{Bmatrix}, \tag{5}$$

where C_{ij} is the elasticity matrix component. The stiffness coefficients are expressed as

$$\begin{aligned} C_{11} &= \frac{E}{1-\nu^2}, \\ C_{12} &= \nu C_{11}, \\ C_{22} &= C_{11}, \\ C_{44} &= C_{55} = C_{66} = \frac{E}{2(1+\nu)}. \end{aligned} \tag{6}$$

2.2 The displacement field of cylindrical shell

According to the first-order shear deformation theory, the displacement fields of SWCNT along the x-, θ-, and z-direction are expressed as

$$\begin{aligned} U(x,\theta,z,t) &= u(x,\theta,t) + z\psi_x(x,\theta,t) \\ V(x,\theta,z,t) &= v(x,\theta,t) + z\psi_\theta(x,\theta,t) \\ W(x,\theta,z,t) &= w(x,\theta,t). \end{aligned} \tag{7}$$

In eq. (7), $u(x,\theta,t)$, $v(x,\theta,t)$, and $w(x,\theta,t)$ are considered as neutral axis displacement, $\psi_\theta(x,\theta,t)$ and $\psi_{\mathrm{x}}(x,\theta,t)$ as the rotation of a transverse normal surface about the circumferential and axial directions.

2.3 Governing equations and boundary conditions

To derive equations of motion and boundary conditions for SWCNT, using the modified couple stress theory and the first-order shear deformation shell model, one must insert the components of displacement field into the strains. Now by substituting the eq. (7) into eqs. (2), (3) and (4), the components of the deviatoric stretch gradient tensor and strain tensor are obtained as follows:

$$\begin{aligned} \varepsilon_{xx} &= \frac{\partial u}{\partial x} + z\frac{\partial \psi_x}{\partial x} \\ \varepsilon_{\theta\theta} &= \frac{1}{R}\frac{\partial v}{\partial \theta} + z\frac{1}{R}\frac{\partial \psi_\theta}{\partial \theta} + \frac{w}{R} \\ \varepsilon_{xz} &= \frac{1}{2}\left(\psi_x + \frac{\partial w}{\partial x}\right) \\ \varepsilon_{x\theta} &= \frac{1}{2}\left(\frac{1}{R}\frac{\partial u}{\partial \theta} + \frac{\partial v}{\partial x}\right) + \frac{z}{2}\left(\frac{1}{R}\frac{\partial \psi_x}{\partial \theta} + \frac{\partial \psi_\theta}{\partial x}\right) \\ \varepsilon_{\theta z} &= \frac{1}{2}\left(\psi_\theta + \frac{1}{R}\frac{\partial w}{\partial \theta} - \frac{v}{R}\right). \end{aligned} \tag{8}$$

Moreover, the non-zero components of symmetric rotation gradient tensor are obtained as follows:

$$\begin{aligned} \chi^s_{xx} &= -\frac{1}{2}\left(\frac{\partial \psi_\theta}{\partial x} + \frac{1}{R}\frac{\partial v}{\partial x} - \frac{1}{R}\frac{\partial^2 w}{\partial x \partial \theta}\right) \\ \chi^s_{\theta\theta} &= -\frac{1}{2R}\left(\frac{1}{R}\frac{\partial u}{\partial \theta} - \frac{\partial v}{\partial x} - z\frac{\partial \psi_\theta}{\partial x}\right) - \frac{1}{2}\left(\frac{1}{R}\frac{\partial^2 w}{\partial x \partial \theta} - \frac{1}{R}\frac{\partial \psi_x}{\partial \theta}\right) \\ \chi^s_{zz} &= -\frac{1}{2}\left(\frac{1}{R}\frac{\partial \psi_x}{\partial \theta} - \frac{\partial \psi_\theta}{\partial x} - \frac{1}{R^2}\frac{\partial u}{\partial \theta}\right) \\ \chi^s_{x\theta} &= -\frac{1}{4}\left(\frac{1}{R^2}\frac{\partial v}{\partial \theta} + \frac{\partial^2 w}{\partial x^2} - \frac{1}{R^2}\frac{\partial^2 w}{\partial \theta^2} - \frac{\partial \psi_x}{\partial x} + \frac{1}{R}\frac{\partial \psi_\theta}{\partial \theta}\right) \\ \chi^s_{xz} &= -\frac{1}{4}\left(\frac{1}{R}\frac{\partial^2 u}{\partial x \partial \theta} - \frac{\partial^2 v}{\partial x^2} - \frac{v}{R^2} + \frac{1}{R^2}\frac{\partial w}{\partial \theta} + \frac{\psi_\theta}{R}\right) - \frac{z}{4}\left(\frac{1}{R}\frac{\partial^2 \psi_\theta}{\partial x \partial \theta} - \frac{\partial^2 \psi_\theta}{\partial x^2}\right) \\ \chi^s_{\theta z} &= -\frac{1}{4}\left(\frac{1}{R^2}\frac{\partial^2 u}{\partial \theta^2} - \frac{1}{R}\frac{\partial^2 v}{\partial x \partial \theta} - \frac{1}{R}\frac{\partial w}{\partial x} + \frac{\psi_x}{R}\right) - \frac{z}{4}\left(\frac{1}{R^2}\frac{\partial^2 \psi_x}{\partial \theta^2} - \frac{1}{R}\frac{\partial^2 \psi_\theta}{\partial x \partial \theta}\right). \end{aligned} \tag{9}$$

For the equations of motion and boundary conditions, the principle of minimum potential energy states that [34]

$$\int_{t_1}^{t_2} (\delta T - \delta U + \delta W - \delta U_h)\mathrm{d}t = 0. \tag{10}$$

The strain energy of SWCNT based on modified couple stress theory is expressed as follows:

$$
\begin{aligned}
\delta U &= \frac{1}{2}\iiint_V (\sigma_{ij}\delta\varepsilon_{ij} + m^s_{ij}\delta\chi^s_{ij})\mathrm{d}V = \delta U_1 + \delta U_2 \\
\delta U_1 &= \frac{1}{2}\iiint_V (\sigma_{ij}\delta\varepsilon_{ij})\mathrm{d}V = \iint_A \left\{ \left(N_{xx}\frac{\partial}{\partial x}\delta u + M_{xx}\frac{\partial}{\partial x}\delta\psi_x \right) + N_{\theta\theta}\left(\frac{1}{R}\frac{\partial}{\partial\theta}\delta v + \frac{\delta w}{R} \right) \right. \\
&\quad + M_{\theta\theta}\frac{1}{R}\frac{\partial}{\partial\theta}\delta\psi_\theta + Q_{xz}\left(\delta\psi_x + \frac{\partial}{\partial x}\delta w \right) \\
&\quad + N_{x\theta}\left(\frac{1}{R}\frac{\partial}{\partial\theta}\delta u + \frac{\partial}{\partial x}\delta v \right) + M_{x\theta}\left(\frac{1}{R}\frac{\partial}{\partial\theta}\delta\psi_x + \frac{\partial}{\partial x}\delta\psi_\theta \right) \\
&\quad \left. + Q_{z\theta}\left(\delta\psi_\theta + \frac{1}{R}\frac{\partial}{\partial\theta}\delta w - \frac{\delta v}{R} \right) \right\} R\,\mathrm{d}x\,\mathrm{d}\theta \\
\delta U_2 &= \frac{1}{2}\iiint_V (m^s_{ij}\delta\chi^s_{ij})\mathrm{d}V = \iint_A \left\{ \left(-\frac{Y_{\theta\theta}}{2R^2} + \frac{Y_{zz}}{2R^2} \right)\frac{\partial}{\partial\theta}\delta u - \left(\frac{Y_{\theta z}}{2R^2} \right)\frac{\partial^2}{\partial\theta^2}\delta u - \left(\frac{Y_{zx}}{2R} \right)\frac{\partial^2}{\partial\theta\partial x}\delta u \right. \\
&\quad + \left(\frac{Y_{\theta\theta}}{2R} - \frac{Y_{xx}}{2R} \right)\frac{\partial}{\partial x}\delta v + \left(\frac{Y_{xz}}{2} \right)\frac{\partial^2}{\partial x^2}\delta v - \left(\frac{Y_{\theta x}}{2R^2} \right)\frac{\partial}{\partial\theta}\delta v \\
&\quad + \left(\frac{Y_{\theta z}}{2R} \right)\frac{\partial^2}{\partial\theta\partial x}\delta v + \left(\frac{Y_{xz}}{2R^2} \right)\delta v + \left(\frac{Y_{\theta z}}{2R} \right)\frac{\partial}{\partial x}\delta w - \left(\frac{Y_{\theta x}}{2} \right)\frac{\partial^2}{\partial x^2}\delta w \\
&\quad - \left(\frac{Y_{zx}}{2R^2} \right)\frac{\partial}{\partial\theta}\delta w + \left(\frac{Y_{x\theta}}{2R^2} \right)\frac{\partial^2}{\partial\theta^2}\delta w + \left(-\frac{Y_{\theta\theta}}{2R} + \frac{Y_{xx}}{2R} \right)\frac{\partial^2}{\partial\theta\partial x}\delta w \\
&\quad + \left(\frac{Y_{x\theta}}{2} \right)\frac{\partial}{\partial x}\delta\psi_x + \left(\frac{Y_{\theta\theta}}{2R} - \frac{Y_{xx}}{2R} \right)\frac{\partial}{\partial\theta}\delta\psi_x - \left(\frac{T_{zx}}{2R} \right)\frac{\partial^2}{\partial\theta\partial x}\delta\psi_x \\
&\quad - \left(\frac{Y_{z\theta}}{2R} \right)\delta\psi_x - \left(\frac{Y_{x\theta}}{2R} \right)\frac{\partial}{\partial\theta}\delta\psi_\theta + \left(\frac{Y_{\theta\theta}}{2R} - \frac{Y_{xx}}{2} + \frac{Y_{zz}}{2} \right)\frac{\partial}{\partial x}\delta\psi_\theta \\
&\quad \left. + \left(\frac{T_{z\theta}}{2R} \right)\frac{\partial^2}{\partial\theta\partial x}\delta\psi_\theta - \left(\frac{T_{z\theta}}{2R^2} \right)\frac{\partial^2}{\partial\theta^2}\delta\psi_x + \left(\frac{T_{xz}}{2} \right)\frac{\partial^2}{\partial x^2}\delta\psi_\theta - \left(\frac{Y_{xz}}{2R} \right)\delta\psi_\theta \right\} R\,\mathrm{d}x\,\mathrm{d}\theta,
\end{aligned}
\tag{11}
$$

where classical and non-classical force and momentum are defined as follows:

$$
\begin{aligned}
(N_{xx}, N_{\theta\theta}, N_{x\theta}) &= \int_{-h/2}^{h/2} (\sigma_{xx}, \sigma_{\theta\theta}, \sigma_{x\theta})\mathrm{d}z, \\
(M_{xx}, M_{\theta\theta}, M_{x\theta}) &= \int_{-h/2}^{h/2} (\sigma_{xx}, \sigma_{\theta\theta}, \sigma_{x\theta}) z\,\mathrm{d}z, \\
(Q_{xz}, Q_{z\theta}) &= \int_{-h/2}^{h/2} k_s(\sigma_{xz}, \sigma_{z\theta})\mathrm{d}z, \\
(Y_{xx}, Y_{\theta\theta}, Y_{zz}, Y_{x\theta}, Y_{xz}, Y_{z\theta}) &= \int_{-h/2}^{h/2} (m_{xx}, m_{\theta\theta}, m_{zz}, m_{x\theta}, m_{xz}, m_{z\theta})\mathrm{d}z, \\
(T_{xx}, T_{\theta\theta}, T_{zz}, T_{x\theta}, T_{xz}, T_{z\theta}) &= \int_{-h/2}^{h/2} (m_{xx}, m_{\theta\theta}, m_{zz}, m_{x\theta}, m_{xz}, m_{z\theta}) z\,\mathrm{d}z.
\end{aligned}
\tag{12}
$$

The velocity vector of any generic point on a rotating shell is expressed as

$$
V = \frac{\partial u}{\partial t} i + \left(\frac{\partial v}{\partial t} + \Omega w \right) j + \left(\frac{\partial w}{\partial t} - \Omega v \right) k. \tag{13}
$$

The first three terms, respectively, are result from linear velocities in axial, circumferential and lateral directions. The fourth and fifth terms are coriolis and centrifugal effects. Overdoted terms represent temporal derivatives. i, j, and k are unit vectors in the x-, θ-, and z-direction, respectively. Furthermore, the kinetic energy of a cylindrical shell can

be expressed as

$$\begin{aligned}\delta T = \int_Z \iint_A \rho\Bigg\{ & \left(\frac{\partial u}{\partial t} + z\frac{\partial \psi_x}{\partial t}\right)\left(\frac{\partial}{\partial t}\delta u + z\frac{\partial}{\partial t}\delta\psi_x\right) + \left(\frac{\partial v}{\partial t} + z\frac{\partial \psi_\theta}{\partial t}\right)\left(\frac{\partial}{\partial t}\delta v + z\frac{\partial}{\partial t}\delta\psi_\theta\right) \\ & + \left(\frac{\partial w}{\partial t}\right)\frac{\partial}{\partial t}\delta w + \Omega\left[w\left(\frac{\partial}{\partial t}\delta v + z\frac{\partial}{\partial t}\delta\psi_\theta\right) - (v + z\psi_\theta)\left(\frac{\partial}{\partial t}\delta w\right)\right. \\ & \left. + \delta w\left(\frac{\partial v}{\partial t} + z\frac{\partial \psi_\theta}{\partial t}\right) - (\delta v + z\delta\psi_\theta)\left(\frac{\partial}{\partial t}w\right)\right] \\ & + \Omega^2\left[(v + z\psi_\theta)(\delta v + z\delta\psi_\theta) + w\delta w\right]\Bigg\} R\,\mathrm{d}z\,\mathrm{d}x\,\mathrm{d}\theta. \end{aligned} \tag{14}$$

The centrifugal force due to rotation produces initial hoop tension. This effect is considered in potential energy. Potential energy involves the non-linear terms of thin Sanders theory in strain relations as recommended [35],

$$U_h = \frac{1}{2}\iint_A N_h\left\{\left(\frac{\partial w}{R\partial\theta} - \frac{v}{R}\right)^2 + \frac{1}{4}\left(\frac{\partial u}{R\partial\theta} - \frac{\partial v}{\partial x}\right)^2\right\} R\,\mathrm{d}\theta\,\mathrm{d}x. \tag{15}$$

In the above equation, $N_h = \rho h R^2\Omega^2$. Also the work done by the surrounding elastic medium can be written as

$$\delta W = \int_0^L \int_0^{2\pi} K_w w\delta w R\,\mathrm{d}\theta\,\mathrm{d}x. \tag{16}$$

Now by substituting eq. (11), eq. (14), eq. (15) and eq. (16) into eq. (10), and integrating by parts, the equations of motion and boundary conditions can be obtained as follows using the first-order shear deformation shell model and modified couple stress theory:

$$\begin{aligned}
&\delta u : \frac{\partial N_{xx}}{\partial x} + \frac{1}{R}\frac{\partial N_{x\theta}}{\partial\theta} + \frac{1}{2R^2}\left(-\frac{\partial Y_{\theta\theta}}{\partial\theta} + \frac{\partial Y_{zz}}{\partial\theta}\right) + \frac{1}{2R}\frac{\partial^2 Y_{zx}}{\partial\theta\partial x} + \frac{1}{2R^2}\frac{\partial^2 Y_{\theta z}}{\partial\theta^2} \\
&- N_h\left(\frac{1}{R}\frac{\partial^2 v}{\partial x\partial\theta} - \frac{1}{R^2}\frac{\partial^2 u}{\partial\theta^2}\right) = I_0\frac{\partial^2 u}{\partial t^2} + I_1\frac{\partial^2\psi_x}{\partial t^2} \\
&\delta v : \frac{\partial N_{x\theta}}{\partial x} + \frac{1}{R}\frac{\partial}{\partial\theta}N_{\theta\theta} + \frac{Q_{z\theta}}{R} + \frac{1}{2}\left\{\frac{1}{R}\frac{\partial}{\partial x}(-Y_{xx} + Y_{\theta\theta}) - \frac{1}{R^2}\frac{\partial Y_{\theta x}}{\partial\theta} - \frac{\partial^2 Y_{xz}}{\partial x^2} - \frac{Y_{xz}}{R^2} - \frac{1}{R}\frac{\partial^2 Y_{z\theta}}{\partial\theta\partial x}\right\} \\
&- N_h\left(\frac{1}{R}\frac{\partial^2 u}{\partial x\partial\theta} - \frac{\partial^2 v}{\partial x^2} + \frac{v}{R^2} - \frac{1}{R^2}\frac{\partial w}{\partial\theta}\right) = I_0\left[\frac{\partial^2 v}{\partial t^2} + 2\left(\frac{\partial w}{\partial t}\right)\Omega - v\Omega^2\right] + I_1\left\{\frac{\partial^2\psi_\theta}{\partial t^2} - \psi_\theta\Omega^2\right\} \\
&\delta w : \frac{\partial Q_{xz}}{\partial x} + \frac{1}{R}\frac{\partial Q_{z\theta}}{\partial\theta} - \frac{N_{\theta\theta}}{R} - \frac{1}{2R^2}\frac{\partial^2 Y_{\theta x}}{\partial\theta^2} - \frac{1}{2R^2}\frac{\partial Y_{zx}}{\partial\theta} + \frac{1}{2R}\frac{\partial Y_{\theta z}}{\partial x} + \frac{\partial^2 Y_{x\theta}}{2\partial x^2} \\
&- \frac{1}{2R}\frac{\partial^2}{\partial\theta\partial x}(Y_{xx} - Y_{\theta\theta}) - N_h\left(\frac{1}{R^2}\frac{\partial v}{\partial\theta} - \frac{1}{R^2}\frac{\partial^2 w}{\partial\theta^2}\right) - K_w w = \\
&I_0\left(\frac{\partial^2 w}{\partial t^2} - 2\Omega\frac{\partial v}{\partial t} - \Omega^2 w\right) - 2I_1\left\{\Omega\frac{\partial\psi_\theta}{\partial t}\right\} \\
&\delta\psi_x : \frac{\partial M_{xx}}{\partial x} + \frac{1}{R}\frac{\partial M_{\theta\theta}}{\partial\theta} - Q_{xz} + \frac{1}{2}\frac{\partial Y_{\theta x}}{\partial x} - \frac{1}{2R}\frac{\partial}{\partial\theta}(Y_{zz} - Y_{\theta\theta}) + \frac{Y_{zz}}{R} + \frac{1}{2R}\frac{\partial^2 T_{zx}}{\partial\theta\partial x} + \frac{1}{2R^2}\frac{\partial^2 T_{\theta z}}{\partial\theta^2} = \\
&I_1\frac{\partial^2 u}{\partial t^2} + I_2\frac{\partial^2\psi_x}{\partial t^2} \\
&\delta\psi_\theta : \frac{1}{R}\frac{\partial M_{\theta\theta}}{\partial\theta} + \frac{\partial M_{x\theta}}{\partial x} - Q_{z\theta} + \frac{1}{2}\frac{\partial}{\partial x}\left(Y_{zz} - Y_{xx} + \frac{T_{\theta\theta}}{R}\right) - \frac{1}{2}\frac{\partial Y_{\theta x}}{\partial\theta} + \frac{Y_{xz}}{2R} - \frac{1}{2R}\frac{\partial^2 T_{\theta z}}{\partial\theta\partial x} - \frac{1}{2}\frac{\partial^2 T_{zx}}{\partial x^2} = \\
&I_1\left(\frac{\partial^2 v}{\partial t^2} + 2\left(\frac{\partial w}{\partial t}\right)\Omega - v\Omega^2\right) + I_2\left(\frac{\partial^2\psi_\theta}{\partial t^2} - \psi_\theta\Omega^2\right).
\end{aligned} \tag{17}$$

Appendix A describes the parameters used in eq. (17). Non-classical boundary conditions are as follows:

$$
\begin{aligned}
\delta u = 0 \quad \text{or} \quad & \left(N_{xx} + \frac{1}{4R}\frac{\partial Y_{xz}}{\partial \theta}\right) n_x + \left(N_{x\theta} - \frac{Y_{\theta\theta} - Y_{zz}}{2R} + \frac{1}{4}\frac{\partial Y_{xz}}{\partial x} + \frac{1}{2R}\frac{\partial Y_{\theta z}}{\partial \theta}\right) n_\theta = 0,\\
\delta u_{,x} = 0 \quad \text{or} \quad & \left(\frac{\partial Y_{xz}}{4}\right) n_\theta = 0,\\
\delta u_{,\theta} = 0 \quad \text{or} \quad & \left(\frac{\partial Y_{xz}}{4}\right) n_x + \left(\frac{\partial Y_{\theta z}}{2}\right) n_\theta = 0,\\
\delta v = 0 \quad \text{or} \quad & \left(N_{x\theta} + \frac{Y_{\theta\theta} - Y_{xx}}{2R} - \frac{1}{2}\frac{\partial Y_{xz}}{\partial x} - \frac{1}{4R}\frac{\partial Y_{\theta z}}{\partial \theta}\right) n_x + \left(N_{\theta\theta} - \frac{1}{4R}\frac{\partial Y_{\theta z}}{\partial x} - \frac{Y_{\theta x}}{2R}\right) n_\theta = 0,\\
\delta v_{,x} = 0 \quad \text{or} \quad & \left(\frac{Y_{zx}}{2}\right) n_x + \left(\frac{Y_{z\theta}}{4}\right) n_\theta = 0,\\
\delta v_{,\theta} = 0 \quad \text{or} \quad & \left(\frac{Y_{z\theta}}{4}\right) n_x = 0,\\
\delta w = 0 \quad \text{or} \quad & \left(Q_{xz} + \frac{Y_{z\theta}}{2R} + \frac{1}{2}\frac{\partial Y_{x\theta}}{\partial x} + \frac{1}{4R}\frac{\partial (Y_{\theta\theta} - Y_{xx})}{\partial \theta}\right) n_x + \left(Q_{\theta z} - \frac{Y_{zx}}{2R} - \frac{1}{2R}\frac{\partial Y_{x\theta}}{\partial \theta} + \frac{1}{4}\frac{\partial (Y_{\theta\theta} - Y_{xx})}{\partial x}\right) n_\theta = 0,\\
\delta w_{,x} = 0 \quad \text{or} \quad & \left(\frac{Y_{x\theta}}{2}\right) n_x + \frac{(Y_{\theta\theta} - Y_{xx})}{4} n_\theta = 0,\\
\delta w_{,\theta} = 0 \quad \text{or} \quad & \frac{(Y_{\theta\theta} - Y_{xx})}{4} n_x + \left(\frac{Y_{x\theta}}{2}\right) n_\theta = 0,\\
\delta \psi_x = 0 \quad \text{or} \quad & \left(M_{xx} + \frac{1}{4R}\frac{\partial T_{xz}}{\partial \theta} + \frac{Y_{x\theta}}{2}\right) n_x + \left(M_{\theta x} + \frac{1}{4}\frac{\partial T_{xz}}{\partial x} + \frac{1}{2R}\frac{\partial T_{\theta z}}{\partial \theta} + \frac{(Y_{\theta\theta} - Y_{zz})}{2}\right) n_\theta = 0,\\
\delta \psi_{x,x} = 0 \quad \text{or} \quad & \left(\frac{T_{xz}}{4}\right) n_\theta = 0,\\
\delta \psi_{x,\theta} = 0 \quad \text{or} \quad & \left(\frac{T_{xz}}{4}\right) n_x + \left(\frac{T_{\theta z}}{2}\right) n_\theta = 0,\\
\delta \psi_\theta = 0 \quad \text{or} \quad & \left(M_{x\theta} - \frac{(Y_{xx} - Y_{zz})}{2} - \frac{1}{4R}\frac{\partial T_{\theta z}}{\partial \theta} - \frac{1}{2}\frac{\partial T_{xz}}{\partial x} + \frac{T_{\theta\theta}}{2R}\right) n_x + \left(M_{\theta\theta} - \frac{Y_{x\theta}}{2} - \frac{1}{4}\frac{\partial T_{\theta z}}{\partial x}\right) n_\theta = 0,\\
\delta \psi_{\theta,x} = 0 \quad \text{or} \quad & \left(\frac{T_{xz}}{2}\right) n_x + \left(\frac{T_{\theta z}}{4}\right) n_\theta = 0,\\
\delta \psi_{\theta,\theta} = 0 \quad \text{or} \quad & \left(\frac{T_{\theta z}}{4}\right) n_x = 0.
\end{aligned}
\tag{18}
$$

3 Solution procedure

Bellman *et al.* introduced the differential quadrature method (DQM) in the early 1970s [36,37] as a reliable and effective method. The number of grid points controls the precision of weighting coefficients, and leads to the accuracy of DQM. In the preliminary formulations of DQM, weighting coefficients were calculated by an algebraic equation system [38, 39]. This limits the number of grid points. Shu [40] devised an explicit formula for the weighting coefficients with the infinite number of grid points, which led to GDQ. The early applications of GDQ have been generally applied to regular domain problems. Shu and Richards [41] developed a domain decomposition technique to be used in the multi-domain problems. By this method, the main domain is divided into a number of sub-domains or elements, before discretizing each sub-domain for GDQ.

The r-th order derivatives of function $f(x_i)$ can be obtained as follows [40]:

$$
\left.\frac{\partial^r f(x)}{\partial x^r}\right|_{x=x_p} = \sum_{j=1}^{n} C_{ij}^{(r)} f(x_i), \tag{19}
$$

where n is the number of grid points along the x-direction, and superscript r is the order of the derivative. Furthermore, C_{ij} is the weighing coefficient, which can be calculated by using the formulations below, for the first-order derivative

along one (x-) direction:

$$C_{ij}^{(1)} = \frac{M(x_i)}{(x_i - x_j)M(x_j)} \quad i,j = 1,2,\ldots,n \text{ and } i \neq j$$
$$C_{ij}^{(1)} = -\sum_{j=1,i\neq j}^{n} C_{ij}^{(1)} \quad i = j, \tag{20}$$

where $M(x)$ is developed as

$$M(x_i) = \prod_{j=1,j\neq i}^{n} (x_i - x_j). \tag{21}$$

In addition, $C^{(r)}$ is obtained by means of the following formulations:

$$C_{ij}^{(r)} = r\left[C_{ij}^{(r-1)}C_{ij}^{(1)} - \frac{C_{ij}^{(r-1)}}{(x_i - x_j)}\right] \quad i,j = 1,2,\ldots,n, i \neq j \text{ and } 2 \leq r \leq n-1$$
$$C_{ii}^{(r)} = -\sum_{j=1,i\neq j}^{n} C_{ij}^{(r)} \quad i,j = 1,2,\ldots,n \text{ and } 1 \leq r \leq n-1. \tag{22}$$

Owing to the geometrical periodicity of the cylindrical shell, displacement vector for free vibration analysis can be described as follows:

$$\begin{Bmatrix} u(x,\theta,t) \\ v(x,\theta,t) \\ w(x,\theta,t) \\ \psi_x(x,\theta,t) \\ \psi_\theta(x,\theta,t) \end{Bmatrix} = \sum_{n=1}^{\infty} \begin{Bmatrix} \bar{u}(x)\cos(n\theta)e^{i\omega t} \\ \bar{v}(x)\sin(n\theta)e^{i\omega t} \\ \bar{w}(x)\cos(n\theta)e^{i\omega t} \\ \bar{\psi}_x(x)\cos(n\theta)e^{i\omega t} \\ \bar{\psi}_\theta(x)\sin(n\theta)e^{i\omega t} \end{Bmatrix}. \tag{23}$$

A proper method to discretize the domain is applying Chebyshev polynomials as it is explained in [42]. Now the following equation is obtained by substituting eq. (23) into eq. (17)

$$\left([M]\{\omega^2\} + [C]\{\omega\} + [K]\right)\begin{pmatrix} d_b \\ d_d \end{pmatrix} = 0. \tag{24}$$

Stiffness matrix $[K]$, damping matrix $[C]$ and mass matrix $[M]$ are obtained by applying GDQ into the equations of motion and the boundary conditions. Moreover, d and b indices denote the domain and boundary, respectively, and d also is the shape of the mode. It is noteworthy that the parameters used in eq. (24) are described in appendix B. For solving eq. (24) and reducing it to the standard form of eigenvalue problem, a convenient way is to rewrite eq. (24) as the following the first-order variable:

$$\left\{\dot{Z}\right\} = \{A\}\{Z\}, \tag{25}$$

in which, state vector Z and state matrix $[A]$ are defined as

$$Z = \begin{Bmatrix} d_d \\ \dot{d}_d \end{Bmatrix} \quad \text{and} \quad [A] = \begin{bmatrix} [0] & [I] \\ -\left[M^{-1}K\right] & -\left[M^{-1}C\right] \end{bmatrix}. \tag{26}$$

In eq. (26), [0] and $[I]$ are the zero and unit (identity) matrices, respectively. Eventually the natural frequency and its mode shape are obtained.

4 Results

The numerical results of the vibration behavior of rotary SWCNT are investigated based on the MCST with considering the initial hoop tension effects for the various boundary conditions. Sufficient number of grid points is necessary to achieve accurate results in GDQ method. As it is shown in table 1, for good results, fifteen grid points are appropriate. The results are shown and analyzed in two sections. The first one compares the proposed model with existing literature. The second section shows the effect of some factors on critical speed and natural frequency of the rotating SWCNT. The said factors are length-to-radius ratio, radius-to-thickness ratio, initial hoop tension, the constant of spring, frequency mode number, angular velocity, material length scale parameter and boundary conditions.

Table 1. The effect of the number of grid points on the results convergence for the non-dimensional natural frequency of the SWCNT with respect to different dimensionless angular velocity and boundary conditions (BCs) when $L/R = 5$, $h/R = 0.2$, $l = R/3$.

Boundary condition	Coefficient of elastic foundation	Angular velocity	$N = 7$	$N = 9$	$N = 11$	$N = 13$	$N = 15$	$N = 17$	$N = 19$
Simply-Simply	$K_W = 10^{18}$	$\Phi = 0.01$	0.22195	0.22193	0.22193	0.22193	0.22193	0.22193	0.22193
	$K_W = 5 \times 10^{18}$	$\Phi = 0.03$	0.24348	0.24345	0.24345	0.24345	0.24345	0.24345	0.24345
Simply-Clamp	$K_W = 10^{18}$	$\Phi = 0.1$	0.24939	0.24939	0.24939	0.24939	0.24939	0.24939	0.24939
	$K_W = 5 \times 10^{18}$	$\Phi = 0.3$	0.26363	0.26363	0.26363	0.26363	0.26363	0.26363	0.26363
Clamp-Clamp	$K_W = 10^{18}$	$\Phi = 0.1$	0.29491	0.29561	0.29550	0.29543	0.29543	0.29543	0.29543
	$K_W = 5 \times 10^{18}$	$\Phi = 0.3$	0.30018	0.30090	0.30079	0.30074	0.30074	0.30074	0.30074
Clamp-Free	$K_W = 10^{18}$	$\Phi = 0.1$	0.13889	0.13850	0.13877	0.13882	0.13882	0.13882	0.13882
	$K_W = 5 \times 10^{18}$	$\Phi = 0.3$	0.17868	0.17839	0.17858	0.17861	0.17862	0.17862	0.17862

Table 2. The material properties of single-walled carbon nanotubes.

E	ν	H	ρ
1.1 Tpa	*0.3*	*0.34* nm	*2300* kg/m^3

Table 3. The comparison of the dimensionless first natural frequencies of non-rotating isotropic homogeneous nanoshells, with simply supported boundary condition and for different thicknesses.

h/R	N	MD simulation [45]	Present GDQM ($l = 0$)	Present Analytical ($l = 0$)	Present GDQM ($l = h$)	Present Analytical ($l = h$)
0.02	1	0.1968	0.1953621557	0.1953621467	0.19543206	0.1954320689
0.05	1	0.2004	0.1954230464	0.1954230557	0.1958578181	0.1958578259

Table 4. The comparison of the dimensionless first three natural frequencies of isotropic homogeneous nanoshells, with simply supported boundary condition and for different thicknesses.

h/R	n	ref. [46] ($l = 0$)	Present study (GDQM) ($l = 0$)	ref. [46] ($l = h$)	Present study (GDQM) ($l = h$)
0.02	1	0.1954	0.19536215	0.1955	0.19543206
	2	0.2532	0.25271274	0.2575	0.25731258
	3	0.2772	0.27580092	0.3067	0.30621690
0.05	1	0.1959	0.19542305	0.1963	0.19585782
	2	0.2623	0.25884786	0.2869	0.28543902
	3	0.3220	0.31407326	0.4586	0.45457555

4.1 Results verification with MD simulation

Carbon nanotubes are often modeled as isotropic elastic cylindrical shells. The anisotropies due to the intrinsic discrete nature of CNTs and imperfections can be neglected because they give a marginal contribution [23]. The material properties of single-walled carbon nanotubes are presented in table 2. The achieved results of MD simulation have been compared with those of GDQ and exact analytical method. Moreover, from tables 3 and 4, it can be clearly seen that by setting $l = h$, the achieved results of the classical theory of cylindrical nanoshells are very close to MD simulation results. Some researchers [43,44] show, as $l = R/3$, the results of the current research based on FSDT are very similar to those of MD simulation. Furthermore, here, dimensionless frequency, is approximated by the equation $\Omega = \omega R\sqrt{\frac{\rho}{E}}$.

Table 5. The comparison of fundamental natural frequency of simply supported SWCNT, for different lengths and elastic foundations when $L/R = 5$, $h = .2R$, $l = R/3$, $n = 1$.

L (nm)	Exact solution $K_w = 10^{18}$	GDQ solution $K_w = 10^{18}$	Exact solution $K_w = 3 \times 10^{18}$	GDQ solution $K_w = 3 \times 10^{18}$	Exact solution $K_w = 6 \times 10^{18}$	GDQ solution $K_w = 6 \times 10^{18}$
1	22.89482103	22.89481960	23.11315206	23.11315064	23.43635032	23.43634892
2	11.50213925	11.50213854	11.71817516	11.71817446	12.03401480	12.03401412
3	7.704384021	7.704383548	7.918192404	7.918191944	8.227111504	8.227111064
4	5.805362478	5.805362125	6.017007402	6.017007062	6.319400017	6.319399696
5	4.665836012	4.665835731	4.875378273	4.875378005	5.171600544	5.171600293
6	3.906058386	3.906058153	4.113555752	4.113555532	4.403930929	4.403930725
7	3.363281181	3.363280990	3.568788612	3.568788426	3.853611243	3.853611073
8	2.956130190	2.363280990	3.159700008	3.159699848	3.439239455	3.439239310
9	2.639397468	2.639397315	2.841079577	2.841079436	3.115582988	3.115582862
10	2.385958257	2.385958114	2.585800272	2.585800147	2.855495111	2.855494999

4.2 The verification of achieved results by using the results of an analytical method

Table 5 shows the GDQ results in comparison with analytical results for different elastic foundations and the lengths of SWCNT. It can be seen, from table 5, that the GDQ results are in accord with analytical results, so the GDQ method with $N = 15$ can be used instead of an analytical solution. Moreover, it can be seen clearly from table 5 that, by increasing the length, natural frequency tends to decrease and it increases when elastic foundation stiffness increases. The comparison of natural frequencies, presented in table 5, shows that an increase in shell length leads to a decrease in the stiffness and, therefore, a decrease in the natural frequency.

4.3 Parametric results

This section investigates the effect of different parameters on the critical speed of rotation and the natural frequency of SWCNT using GDQM and MCST.

4.3.1 The effect of circumferential wave number on natural frequency for different boundary conditions, elastic foundation, and the different values of angular velocity

Table 6 gives a presentation of circumferential wave numbers, angular velocity, and elastic foundation effect on natural frequency under the various boundary conditions. As it can be seen from table 6, an increase in Winkler foundation leads to an increase in the frequency of all modes. This trend is observed under all types of boundary conditions. This is because increasing the Winkler foundation is eventuated to increase in stiffness and natural frequency of the rotating SWCNT. In addition, the increase in the modes of the frequency results in considerable increase in natural frequency. Clamped-Free boundary condition has the lowest frequency because of its particular condition, and Clamp-Clamp boundary condition has the highest frequency. Also it can be seen from the table 6 that in fundamental frequency, the increase in angular speed leads to the decrease in the frequency. A surprising result is that unlike C-C, C-S, and S-S boundary, under C-F boundary condition, an increase in rotational speed results in a decrease in the second frequency mode as the same as first frequency mode. In the third frequency, an increase in rotational speed leads to an increase in frequency. This happens under all types of boundary condition.

4.3.2 The effect of different Winkler foundations on the natural frequency and the critical speed of rotation for different boundary conditions

Figure 3 demonstrates natural frequency *versus* angular velocity for a nanotube on different Winkler foundations. The figure shows that an increase in Winkler stiffness coefficient increases the critical speed of rotation and causes an increase in stability of carbon nanotube. This is because of the fact that an increase in Winkler stiffness coefficient leads to an increase in the stiffness of carbon nanotube, and causes natural frequency and stability to increase. Figure 4 to 6 present a similar trend. When one draws a comparison between figs. 3, 4, 5, and 6, it can be inferred that while a boundary condition changes from free to simply and from simply to clamp both natural frequencies and angular velocities increase. This results in an increase in the stability of carbon nanotubes.

Table 6. The variation of the fundamental, the second and the third frequency (THz), *versus* different Winkler stiffness of a rotating carbon nanotube for different angular velocities (THz) and boundary conditions when $L/R = 5$, $h/R = 0.2$ and $l = R/3$.

	Fundamental frequency			Second frequency			Third frequency		
	$\phi = 0$	0.3	0.5	$\phi = 0$	0.3	0.5	$\phi = 0$	0.3	0.5
Simply-Simply									
K_w									
0	1.96420	1.92414	1.85033	4.95947	4.96075	4.96296	12.4342	12.4488	12.4749
1×10^{18}	2.07125	2.03346	1.96405	5.02470	5.02596	5.02815	12.4625	12.7472	12.5031
3×10^{18}	2.26824	2.23408	2.17162	5.15238	5.15362	5.15577	12.5190	12.5336	12.5594
5×10^{18}	2.44695	2.41559	2.35844	5.27657	5.27780	5.27991	15.5751	12.5896	12.6153
Simply-Clamp									
K_w									
0	2.34960	2.31363	2.25292	5.13716	5.13853	5.14094	12.5145	12.5291	12.5552
1×10^{18}	2.44026	2.40841	2.35039	5.20087	5.20223	5.20461	12.5428	12.5575	12.5835
3×10^{18}	2.61532	2.58587	2.53237	5.32573	5.32706	5.32941	12.5994	12.6139	12.6398
5×10^{18}	2.77725	2.74977	2.69994	5.44736	5.44868	5.45098	12.6556	12.6700	12.6957
Clamp-Clamp									
K_w									
0	2.78211	2.75371	2.70227	5.37941	5.38090	5.38356	12.9229	12.9376	12.9637
1×10^{18}	2.86646	2.83899	2.78928	5.44165	5.44312	5.44577	12.6514	12.6661	12.6922
3×10^{18}	3.02698	3.00114	2.95444	5.56382	5.56528	5.56788	12.7083	12.7229	12.7489
5×10^{18}	3.17796	3.15350	3.10937	5.68309	5.68452	5.68709	12.7649	12.7794	12.8053
Clamp-Free									
K_w									
0	1.18091	1.1010	0.94691	4.92642	4.92341	4.92247	12.3212	12.3326	12.3570
1×10^{18}	1.36092	1.29186	1.16324	4.99503	4.99198	4.99101	12.3508	12.3622	12.3865
3×10^{18}	1.66123	1.60475	1.50318	5.12926	5.12615	5.12512	12.4098	12.4211	12.4452
5×10^{18}	1.91235	1.86327	1.77667	5.25978	5.25660	5.25550	12.4684	12.4797	12.5036

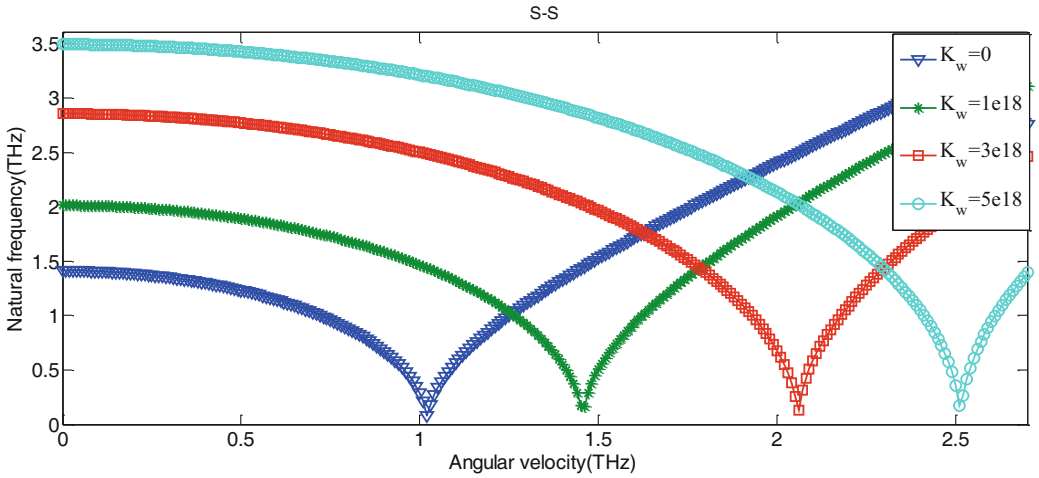

Fig. 3. The variation of fundamental frequency (THz) *versus* the angular velocity of a rotating Simply-Simply SWCNT with different Winkler foundations when $l = R/3$, $L = 10 * R$ and $h = 0.1R$.

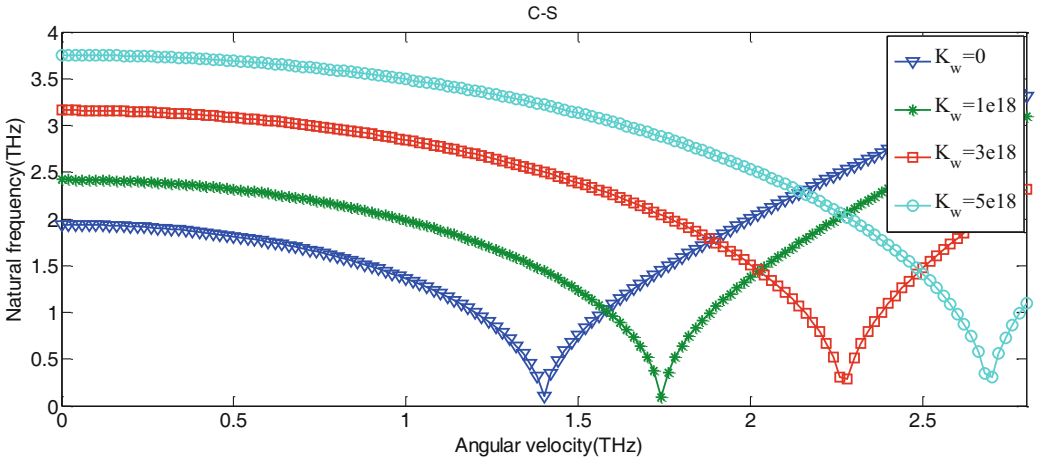

Fig. 4. The variation of fundamental frequency (THz) *versus* the angular velocity of a rotating Clamp-Simply SWCNT with different Winkler foundations when $l = R/3$, $L = 10 * R$ and $h = 0.1R$.

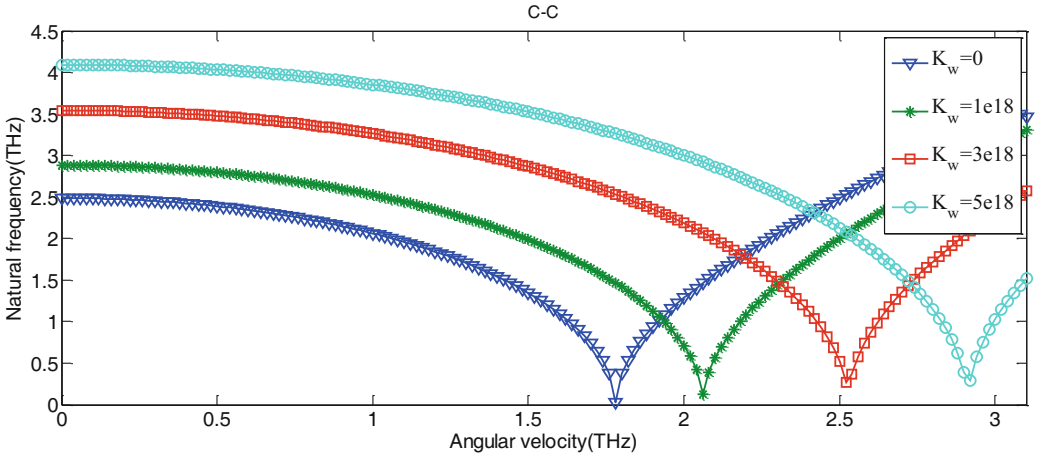

Fig. 5. The variation of fundamental frequency (THz) *versus* the angular velocity of a rotating Clamp-Clamp SWCNT with different Winkler foundations when $l = R/3$, $L = 10 * R$ and $h = 0.1R$.

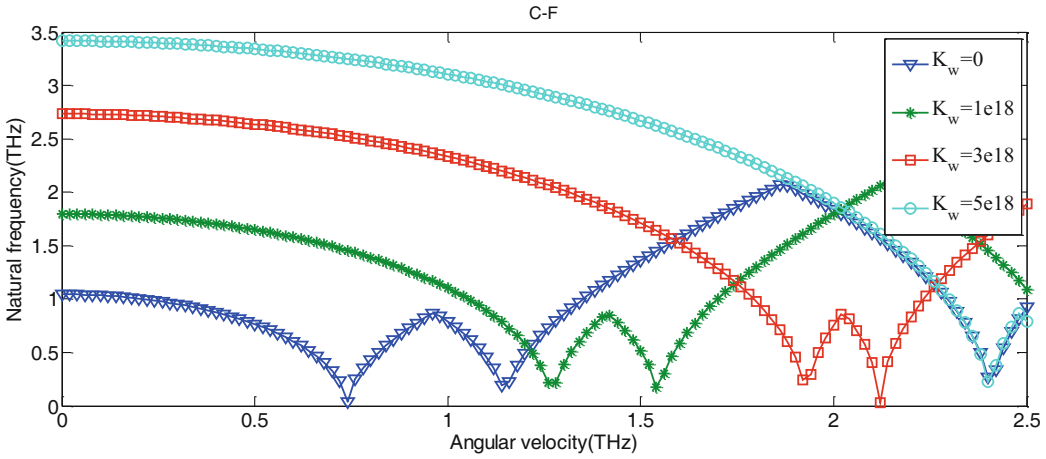

Fig. 6. The variation of fundamental frequency (THz) *versus* the angular velocity of a rotating Clamp-Free SWCNT with different Winkler foundations when $l = R/3$, $L = 10 * R$ and $h = 0.1R$.

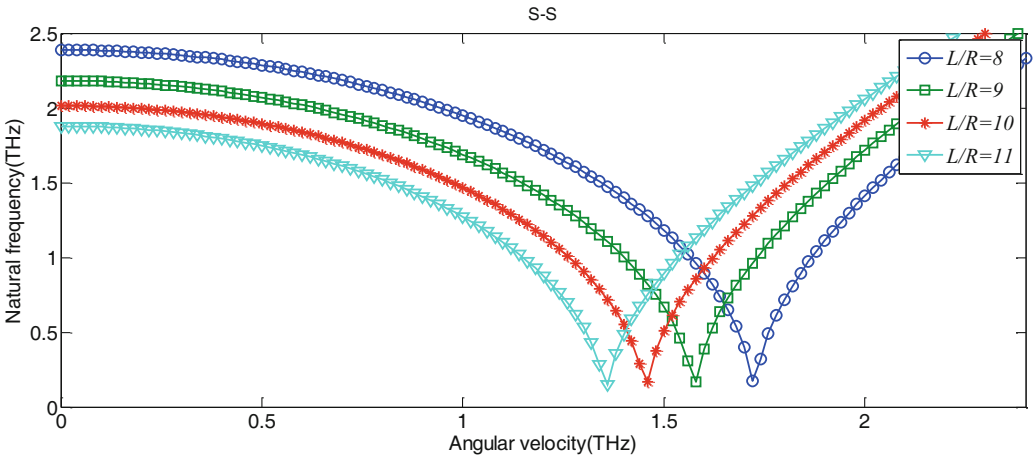

Fig. 7. The variation of fundamental frequency (THz) *versus* the angular velocity of a rotating Simply-Simply SWCNT with different length-to-radius ratios when $h/R = 0.1$ and $l = R/3$.

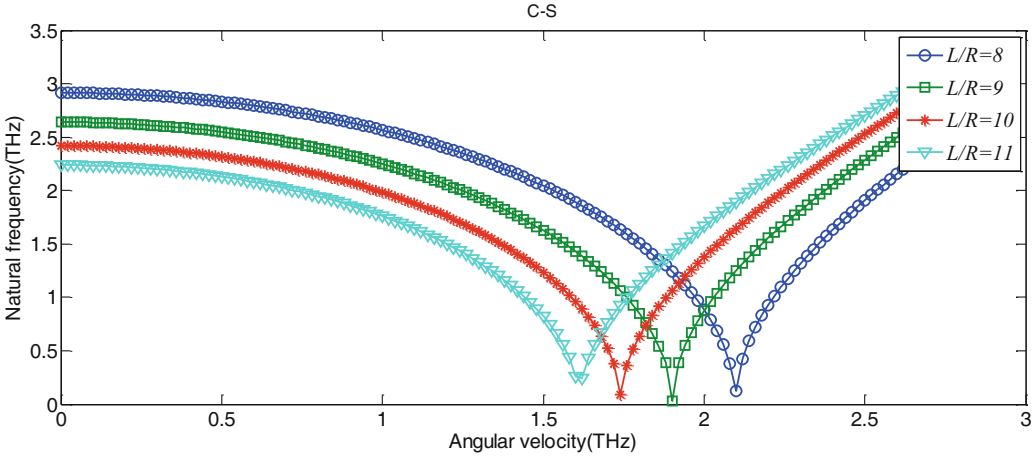

Fig. 8. The variation of fundamental frequency (THz) *versus* the angular velocity of a rotating Clamp-Simply SWCNT with different length-to-radius ratios when $h/R = 0.1$ and $l = R/3$.

4.3.3 The effect of different length-to-radius ratios on the natural frequency and the critical speed of rotation for different boundary conditions

Figure 7 shows natural frequency *versus* angular velocity for different length-to-radius ratios. It can be seen from the graph that as the length-to-radius ratio increases, the critical speed of rotation decreases, this leads to an increase in the instability of carbon nanotube. This effect is more significant in lower angular velocities. This trend also is deduced from figs. 8 to 10. When figs. 7 to 10 are compared with each other, it can be inferred that while a boundary condition changes from free to simply and from simply to clamp both natural frequencies and angular velocities increase. This results in an increase in the stability of carbon nanotubes.

4.3.4 The effect of different material length scale parameters on the natural frequency and the critical speed of rotation for different boundary conditions

Figure 11 presents natural frequency *versus* angular velocity for different material length scale parameters. It can be seen from the graph that an increase in the material length parameter leads to an increase in the critical speed of rotation. This increase is more significant in lower angular velocities. This increases the stability of the carbon nanotube. Figures 12 to 14 show the same behavior as in fig. 11. When the comparison between figs. 11, 12, 13, and 14 is taken into account, it can be deduced that while a boundary condition changes from free to simply and from simply to clamp both natural frequencies and angular velocities increase. This results in an increase in the stability of carbon nanotubes.

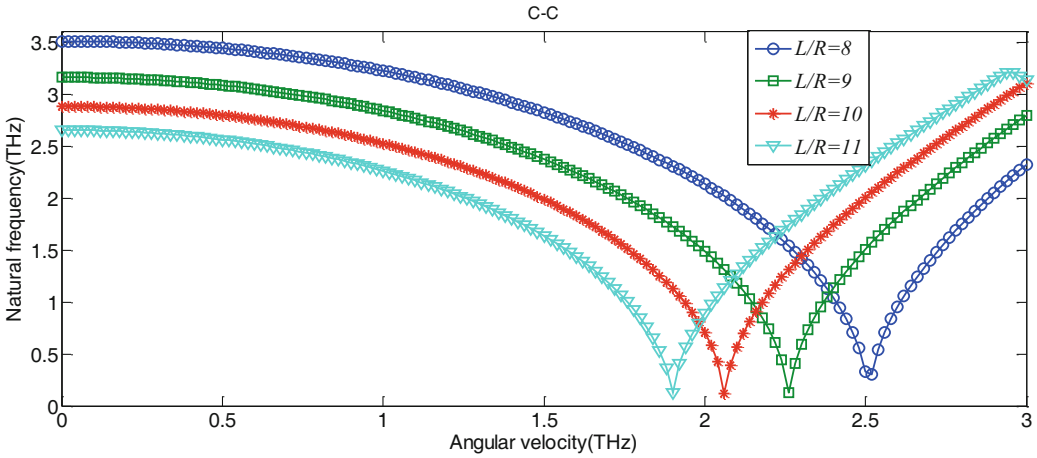

Fig. 9. The variation of fundamental frequency (THz) *versus* theangular velocity of a rotating Clamp-Clamp SWCNT with different length-to-radius ratios when $h/R = 0.1$ and $l = R/3$.

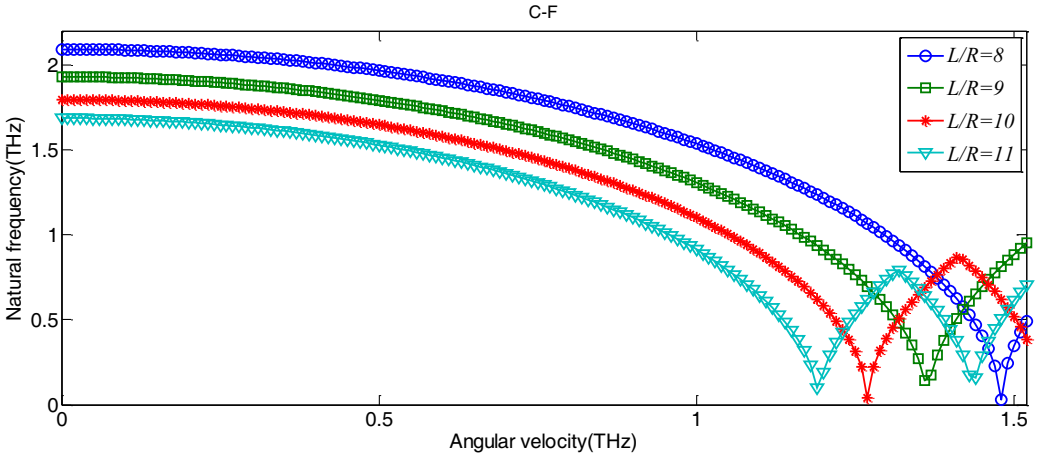

Fig. 10. The variation of fundamental frequency (THz) *versus* the angular velocity of a rotating Clamp-Free SWCNT with different length-to-radius ratios when $h/R = 0.1$ and $l = R/3$.

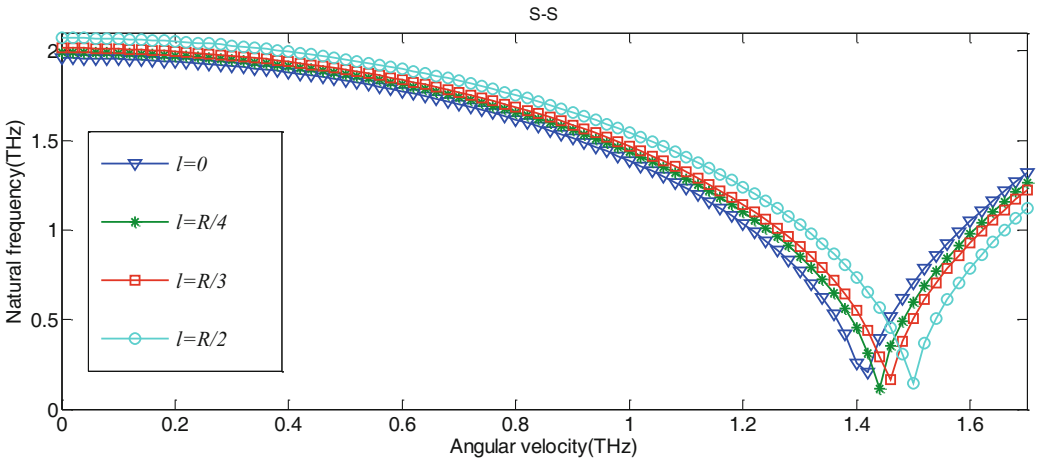

Fig. 11. The variation of fundamental frequency (THz) *versus* the angular velocity of a rotating Simply-Simply SWCNT with different length scale parameters when $h/R = 0.1$ and $L = 10\,\text{nm}$.

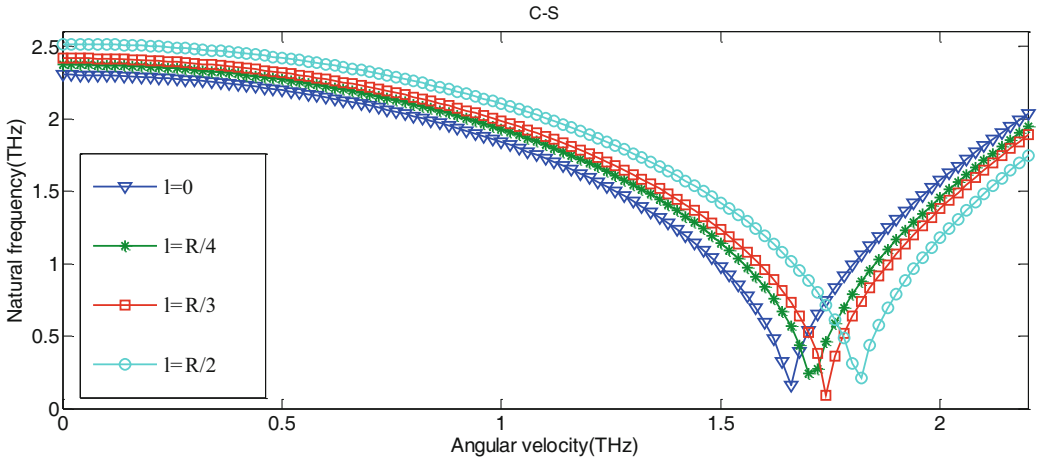

Fig. 12. The variation of fundamental frequency (THz) *versus* the angular velocity of a rotating Clamp-Simply SWCNT with different length scale parameters when $h/R = 0.1$ and $L = 10\,\text{nm}$.

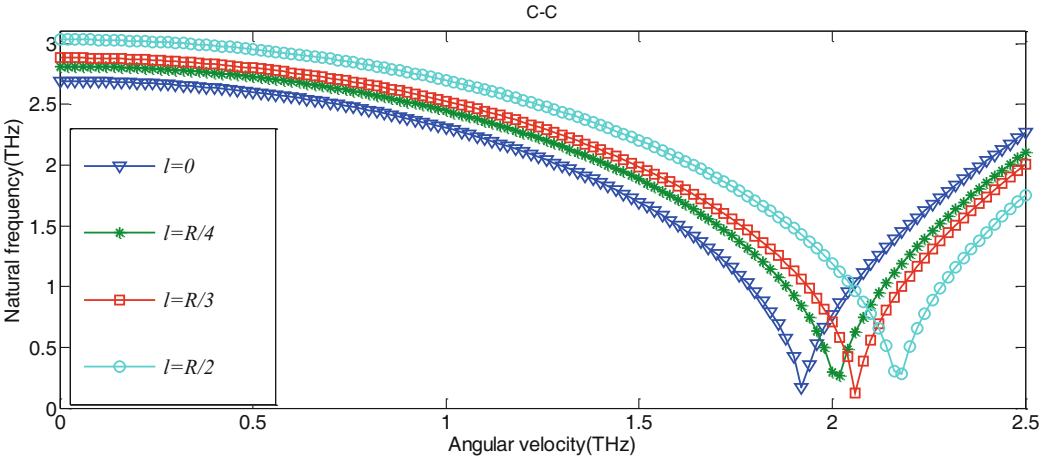

Fig. 13. The variation of fundamental frequency (THz) *versus* the angular velocity of a rotating Clamp-Clamp SWCNT with different length scale parameters when $h/R = 0.1$ and $L = 10\,\text{nm}$.

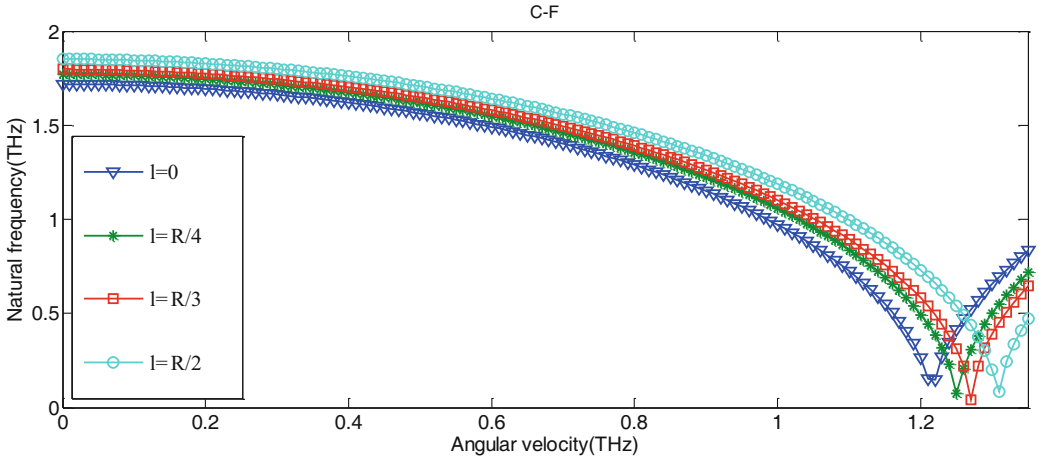

Fig. 14. The variation of fundamental frequency (THz) *versus* the angular velocity of a rotating Clamp-Free SWCNT with different length scale parameters when $h/R = 0.1$ and $L = 10\,\text{nm}$.

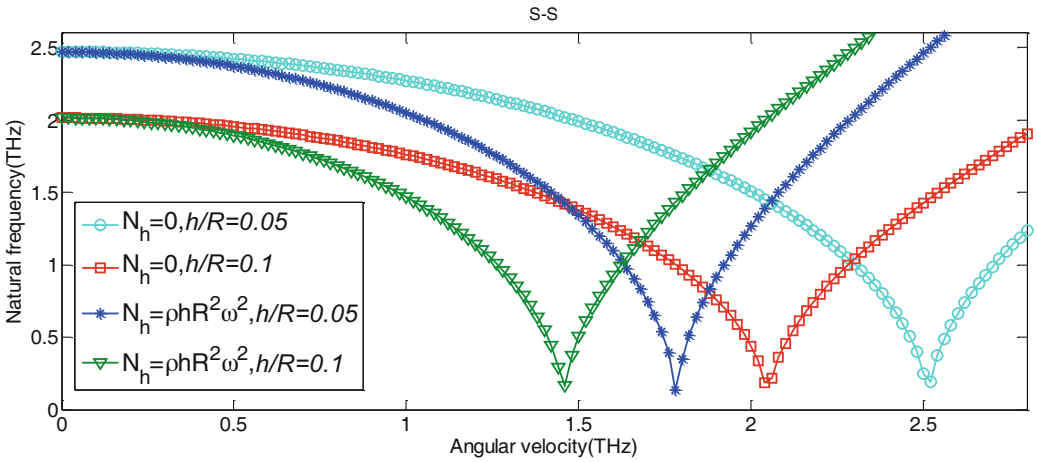

Fig. 15. The variation of fundamental frequency (THz) *versus* the angular velocity of a rotating Simply-Simply SWCNT with different initial hoop tensions and thickness-to-radius ratio parameters when $l = R/3$, $L = 10 * R$ and $L = 10\,\text{nm}$.

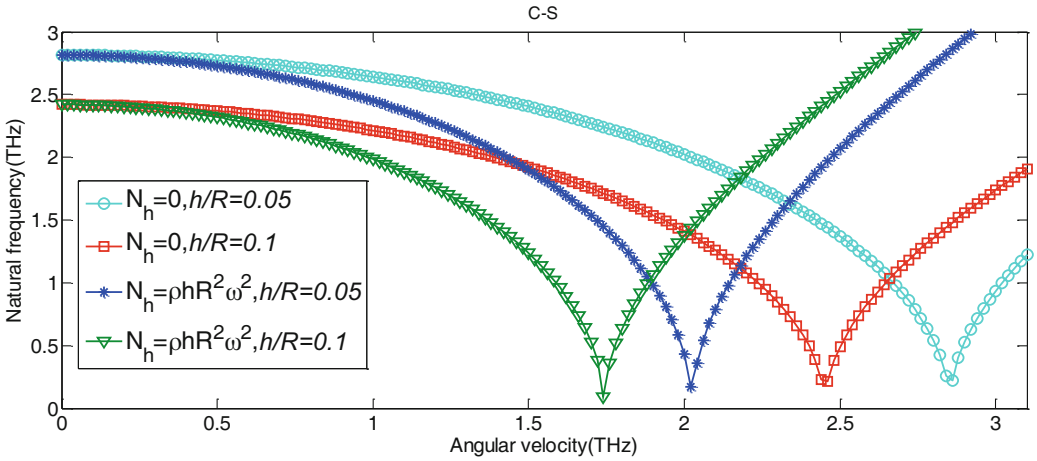

Fig. 16. The variation of fundamental frequency (THz) *versus* the angular velocity of a rotating Clamp-Simply SWCNT with different initial hoop tensions and thickness-to-radius ratio parameters when $l = R/3$, $L = 10 * R$ and $L = 10\,\text{nm}$.

4.3.5 The effect of different initial hoop tensions and thickness-to-radius ratios on the natural frequency and the critical speed of rotation for different boundary conditions

Figure 15 illustrates natural frequency *versus* angular velocity for different thickness-to-radius ratios. It can be seen, from fig. 15, that an increase in the thickness-to-radius ratio causes an increase in the critical speed of rotation and increases the stability of carbon nanotubes. Moreover, when the initial hoop tension changes from zero to $\rho h R^2 \omega^2$, the critical speed of rotation decreases and leads to a decrease in the stability of carbon nanotubes. This change plays a more noticeable role at a higher speed of rotation. This trend is also deduced from figs. 16 to 18. When figs. 15 to 18 are compared with each other, it can be inferred that while a boundary condition changes from free to simply and from simply to clamp, both natural frequencies and angular velocities increase, so carbon nanotubes become more stable.

5 Conclusion

This article presents the size-dependent vibration analysis of a rotating SWCNT, and obtains the critical angular velocity of the rotating SWCNT. Modified couple stress theory introduces size-dependent effects. The equations of motion and non-classic boundary conditions are derived using the Hamilton principle. The natural frequency of the rotating SWCNT is investigated regarding material length scale parameter, angular velocity, length, length-to-radius

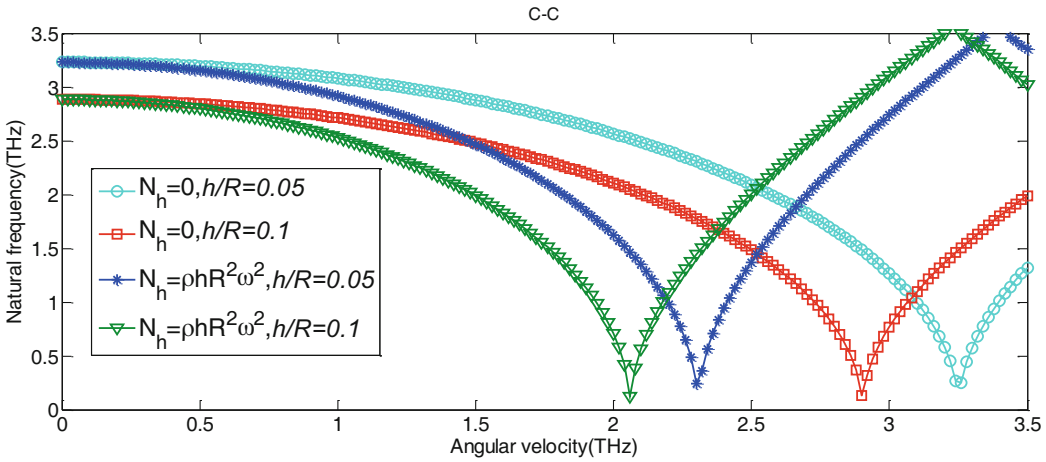

Fig. 17. The variation of fundamental frequency (THz) *versus* the angular velocity of a rotating Clamp-Clamp SWCNT with different initial hoop tensions and thickness-to-radius ratio parameters when $l = R/3$, $L = 10 * R$ and $L = 10\,\text{nm}$.

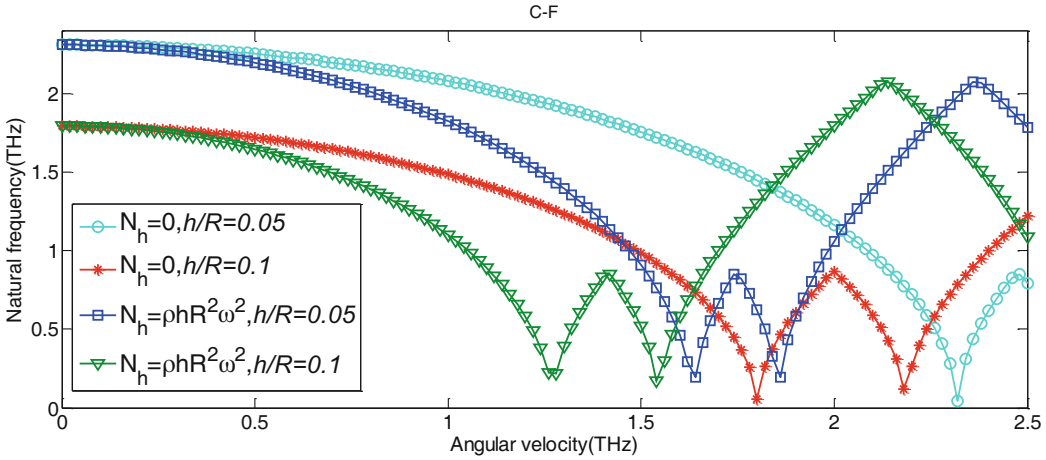

Fig. 18. The variation of fundamental frequency (THz) *versus* the angular velocity of a rotating Clamp-Free SWCNT with different initial hoop tensions and thickness-to-radius ratio parameters when $l = R/3$, $L = 10 * R$ and $L = 10\,\text{nm}$.

ratio, radius-to-thickness ratio, initial hoop tension, and boundary conditions on critical speed of a rotating SWCNT. In this study, the following main results can be achieved:

1) With an increase in the length-to-radius ratio and material length scale parameter, the natural frequency tends to increase while an increase in the angular velocity results in a decrease in the natural frequency of the rotating SWCNT.
2) Clamp-Free boundary condition has the lowest natural frequency because of its particular condition, while the Clamp-Clamp boundary condition has the highest natural frequency.
3) The results show that an increase in the material length scale parameter leads to an increase in the critical speed, while an increase in the length-to-radius ratio of the rotating SWCNT.
4) The results show that the initial hoop tension plays an important role in the critical speed of a rotating SWCNT so that, by ignoring this effect, the critical velocity increases.

Appendix A.

$$N_{xx} = A_{11}\frac{\partial u}{\partial x} + B_{11}\frac{\partial \psi_x}{\partial x} + A_{12}\left(\frac{\partial v}{R\partial\theta} + \frac{w}{R}\right) + B_{12}\frac{\partial \psi_\theta}{R\partial\theta},$$

$$Q_{xz} = k_s A_{55}\left(\psi_x + \frac{\partial w}{\partial x}\right),$$

$$N_{\theta\theta} = A_{11}\left(\frac{w}{R} + \frac{1}{R}\frac{\partial v}{\partial \theta}\right) + B_{11}\frac{1}{R}\frac{\partial \psi_\theta}{\partial \theta} + A_{12}\frac{\partial u}{\partial x} + B_{12}\frac{\partial \psi_x}{\partial x}$$

$$Q_{z\theta} = k_s A_{55}\left(\psi_\theta + \frac{1}{R}\frac{\partial w}{\partial \theta} - \frac{v}{R}\right),$$

$$N_{x\theta} = A_{55}\left(\frac{1}{R}\frac{\partial u}{\partial \theta} + \frac{\partial v}{\partial x}\right) + B_{55}\left(\frac{1}{R}\frac{\partial \psi_x}{\partial \theta} + \frac{\partial \psi_\theta}{\partial x}\right),$$

$$M_{xx} = B_{11}\frac{\partial u}{\partial x} + D_{11}\frac{\partial \psi_x}{\partial x} + B_{12}\left(\frac{\partial v}{R\partial \theta} + \frac{w}{R}\right) + D_{12}\frac{\partial \psi_\theta}{R\partial \theta},$$

$$M_{\theta\theta} = B_{11}\left(\frac{w}{R} + \frac{1}{R}\frac{\partial v}{\partial \theta}\right) + D_{11}\frac{1}{R}\frac{\partial \psi_\theta}{\partial \theta} + B_{12}\frac{\partial u}{\partial x} + D_{12}\frac{\partial \psi_x}{\partial x},$$

$$M_{x\theta} = B_{55}\left(\frac{1}{R}\frac{\partial u}{\partial \theta} + \frac{\partial v}{\partial x}\right) + D_{55}\left(\frac{1}{R}\frac{\partial \psi_x}{\partial \theta} + \frac{\partial \psi_\theta}{\partial x}\right),$$

$$Y_{xx} = -A_{55}l^2\left(\frac{\partial \psi_\theta}{\partial x} + \frac{1}{R}\frac{\partial v}{\partial x} - \frac{1}{R}\frac{\partial^2 w}{\partial x \partial \theta}\right),$$

$$Y_{\theta\theta} = -A_{55}l^2\left[\frac{1}{R}\left(\frac{1}{R}\frac{\partial u}{\partial \theta} - \frac{\partial v}{\partial x}\right) + \frac{1}{R}\frac{\partial^2 w}{\partial x \partial \theta} - \frac{1}{R}\frac{\partial \psi_x}{\partial \theta}\right] - B_{55}l^2\left(-\frac{\partial \psi_\theta}{\partial x}\right),$$

$$Y_{zz} = -A_{55}l^2\left[-\frac{1}{R^2}\frac{\partial u}{\partial \theta} + \frac{1}{R}\frac{\partial \psi_x}{\partial \theta} - \frac{\partial \psi_\theta}{\partial x}\right],$$

$$Y_{x\theta} = -\frac{A_{55}l^2}{2}\left(\frac{1}{R^2}\frac{\partial v}{\partial \theta} + \frac{\partial^2 w}{\partial x^2} - \frac{1}{R^2}\frac{\partial^2 w}{\partial \theta^2} + \frac{1}{R}\frac{\partial \psi_\theta}{\partial \theta} - \frac{\partial \psi_x}{\partial x}\right),$$

$$Y_{xz} = -\frac{A_{55}l^2}{2}\left[-\frac{\partial^2 v}{\partial x^2} - \frac{v}{R^2} + \frac{1}{R}\frac{\partial^2 u}{\partial x \partial \theta} + \frac{\psi_\theta}{R} + \frac{1}{R^2}\frac{\partial w}{\partial \theta}\right] - \frac{B_{55}l^2}{2}\left(\frac{1}{R}\frac{\partial^2 \psi_x}{\partial x \partial \theta} - \frac{\partial^2 \psi_\theta}{\partial x^2}\right),$$

$$Y_{\theta z} = -\frac{A_{55}l^2}{2}\left[\frac{1}{R^2}\frac{\partial^2 u}{\partial \theta^2} - \frac{1}{R}\frac{\partial^2 v}{\partial x \partial \theta} + \frac{\psi_x}{R} - \frac{1}{R}\frac{\partial w}{\partial x}\right] - \frac{B_{55}l^2}{2}\left(\frac{1}{R^2}\frac{\partial^2 \psi_x}{\partial \theta^2} - \frac{1}{R}\frac{\partial^2 \psi_\theta}{\partial x \partial \theta}\right),$$

$$T_{xz} = -\frac{B_{55}l^2}{2}\left[-\frac{\partial^2 v}{\partial x^2} - \frac{v}{R^2} + \frac{1}{R}\frac{\partial^2 u}{\partial x \partial \theta} + \frac{\psi_\theta}{R} + \frac{1}{R^2}\frac{\partial w}{\partial \theta}\right] - \frac{D_{55}l^2}{2}\left(\frac{1}{R}\frac{\partial^2 \psi_x}{\partial x \partial \theta} - \frac{\partial^2 \psi_\theta}{\partial x^2}\right),$$

$$T_{\theta z} = -\frac{B_{55}l^2}{2}\left[\frac{1}{R^2}\frac{\partial^2 u}{\partial \theta^2} - \frac{1}{R}\frac{\partial^2 v}{\partial x \partial \theta} + \frac{\psi_x}{R} - \frac{1}{R}\frac{\partial w}{\partial x}\right] - \frac{D_{55}l^2}{2}\left(\frac{1}{R^2}\frac{\partial^2 \psi_x}{\partial \theta^2} - \frac{1}{R}\frac{\partial^2 \psi_\theta}{\partial x \partial \theta}\right),$$

$$T_{\theta\theta} = -B_{55}l^2\left[\frac{1}{R}\left(\frac{1}{R}\frac{\partial u}{\partial \theta} - \frac{\partial v}{\partial x}\right) + \frac{1}{R}\frac{\partial^2 w}{\partial x \partial \theta} - \frac{1}{R}\frac{\partial \psi_x}{\partial \theta}\right] - D_{55}l^2\left(-\frac{\partial \psi_\theta}{\partial x}\right),$$

Appendix B.

$$K_{11} = \left\{A_{11}\sum_{k=1}^{i} C_{i,k}^{(2)} - A_{55}\left(\frac{n}{R}\right)^2 + \frac{A_{55}l^2n^2}{4R^2}\sum_{k=1}^{i} C_{i,k}^{(2)} + \left(-\frac{A_{55}l^2n^4}{4R^4}\right) - \frac{A_{55}l^2n^2}{R^4} - N_h\frac{n^2}{R^2}\right\}\bar{u},$$

$$K_{12} = \left\{\frac{A_{12}n}{R}\sum_{k=1}^{i} C_{i,k}^{(1)} + \frac{A_{55}n}{R}\sum_{k=1}^{i} C_{i,k}^{(1)} + \frac{A_{55}l^2n}{4R}\sum_{k=1}^{i} C_{i,k}^{(3)} + \left(\frac{A_{55}l^2(-n-n^3)}{4R^3}\right)\sum_{k=1}^{i} C_{i,k}^{(1)} - \frac{N_hn}{4R}\sum_{k=1}^{i} C_{i,k}^{(1)}\right\}\bar{v},$$

$$K_{13} = \left\{\frac{A_{12}}{R}\sum_{k=1}^{i} C_{i,k}^{(1)} - \left(\frac{A_{55}l^2n^2}{2R^3}\right)\sum_{k=1}^{i} C_{i,k}^{(1)}\right\}\bar{w},$$

$$K_{14} = \left\{B_{11}\sum_{k=1}^{i} C_{i,k}^{(2)} - B_{55}\frac{n^2}{R^2} + \frac{B_{55}l^2n^2}{4R^2}\sum_{k=1}^{i} C_{i,k}^{(2)} + \left(\frac{5A_{55}l^2n^2}{4R^3} - \frac{B_{55}l^2n^4}{4R^4}\right)\right\}\bar{\psi}_x,$$

$$K_{15} = \left\{\frac{B_{12}n}{R}\sum_{k=1}^{i} C_{i,k}^{(1)} + \frac{B_{55}n}{R}\sum_{k=1}^{i} C_{i,k}^{(1)} + \frac{B_{55}l^2n}{4R}\sum_{k=1}^{i} C_{i,k}^{(3)} - \left(\frac{(B_{55})l^2n}{2R^3} + \frac{A_{55}l^2n}{4R^2} - \frac{B_{55}l^2n^3}{4R^3}\right)\sum_{k=1}^{i} C_{i,k}^{(1)}\right\}\bar{\psi}_\theta,$$

$$K_{21} = -\left\{+\frac{A_{12}n}{R}\sum_{k=1}^{i}C_{i,k}^{(1)} + \frac{A_{55}n}{R}\sum_{k=1}^{i}C_{i,k}^{(1)} + \frac{A_{55}l^2n}{4R}\sum_{k=1}^{i}C_{i,k}^{(3)} + \left(\frac{A_{55}l^2(-n-n^3)}{4R^3}\right)\sum_{k=1}^{i}C_{i,k}^{(1)} - \frac{N_hn}{4R}\sum_{k=1}^{i}C_{i,k}^{(1)}\right\}\bar{u},$$

$$K_{22} = \left\{A_{55}\sum_{k=1}^{i}C_{i,k}^{(2)} - A_{11}\left(\frac{n}{R}\right)^2 - \frac{k_sA_{55}}{R^2} - \frac{A_{55}l^2}{4}\sum_{k=1}^{i}C_{i,k}^{(4)} + \left(\frac{A_{55}l^2(2+n^2)}{4R^2}\right)\sum_{k=1}^{i}C_{i,k}^{(2)} + \frac{N_h}{R^2} + I_0\Omega^2 + \left(-\frac{A_{55}l^2(1+n^2)}{4R^4}\right) + \frac{N_h}{4}\sum_{k=1}^{i}C_{i,k}^{(2)}\right\}\bar{v},$$

$$K_{23} = \left\{-A_{11}\frac{n}{R^2} - k_sA_{55}\frac{n}{R^2} + \left(\frac{A_{55}l^2n}{4R^2}\right)\sum_{k=1}^{i}C_{i,k}^{(2)} + \left(-\frac{A_{55}l^2(n^3+n)}{4R^4}\right) - \frac{N_hn}{R^2}\right\}\bar{w},$$

$$K_{24} = \left\{-\frac{B_{55}n}{R}\sum_{k=1}^{i}C_{i,k}^{(1)} - \frac{B_{12}n}{R}\sum_{k=1}^{i}C_{i,k}^{(1)} - \frac{B_{55}l^2n}{4R}\sum_{k=1}^{i}C_{i,k}^{(3)} - \left(\frac{A_{55}l^2n}{2R^2} + \frac{B_{55}l^2(-n^3+n)}{4R^3}\right)\sum_{k=1}^{i}C_{i,k}^{(1)}\right\}\bar{\psi}_x,$$

$$K_{25} = \left\{B_{55}\sum_{k=1}^{i}C_{i,k}^{(2)} - B_{11}\left(\frac{n}{R}\right)^2 + \frac{k_sA_{55}}{R} - \frac{B_{55}l^2}{4}\sum_{k=1}^{i}C_{i,k}^{(4)} - \left(\frac{-3A_{55}l^2}{4R} - \frac{B_{55}l^2}{2R} - \frac{B_{55}l^2(n^2-1)}{4R^2}\right)\sum_{k=1}^{i}C_{i,k}^{(2)} + \left(\frac{A_{55}l^2(1-n^2)}{4R^3}\right) + I_1\Omega^2\right\}\bar{\psi}_\theta,$$

$$K_{31} = -\left\{+\frac{A_{12}}{R}\sum_{k=1}^{i}C_{i,k}^{(1)} - \left(\frac{A_{55}l^2n^2}{2R^3}\right)\sum_{k=1}^{i}C_{i,k}^{(1)}\right\}\bar{u},$$

$$K_{32} = \left\{-A_{11}\frac{n}{R^2} - k_sA_{55}\frac{n}{R^2} + \left(\frac{A_{55}l^2n}{4R^2}\right)\sum_{k=1}^{i}C_{i,k}^{(2)} + \left(-\frac{A_{55}l^2(n^3+n)}{4R^4}\right) - \frac{N_hn}{R^2}\right\}\bar{v},$$

$$K_{33} = \left\{k_sA_{55}\sum_{k=1}^{i}C_{i,k}^{(2)} - k_sA_{55}\left(\frac{n}{R}\right)^2 - \frac{A_{11}}{R^2} - \frac{A_{55}l^2}{4}\sum_{k=1}^{i}C_{i,k}^{(4)} - K_w + \left(\frac{A_{55}l^2(2n^2+1)}{4R^2}\right)\sum_{k=1}^{i}C_{i,k}^{(2)} - \frac{A_{55}l^2(n^2+n^4)}{4R^4} - N_h\frac{n^2}{R^2} + I_0\Omega^2\right\}\bar{w},$$

$$K_{34} = \left\{k_sA_{55}\sum_{k=1}^{i}C_{i,k}^{(1)} - \frac{B_{12}}{R}\sum_{k=1}^{i}C_{i,k}^{(1)} + \frac{A_{55}l^2}{4}\sum_{k=1}^{i}C_{i,k}^{(3)} - \left(\frac{A_{55}l^2(n^2+1)}{4R^2}\right)\sum_{k=1}^{i}C_{i,k}^{(1)}\right\}\bar{\psi}_x,$$

$$K_{35} = \left\{\frac{k_sA_{55}n}{R} - \frac{B_{11}n}{R^2} + \left(\frac{B_{55}l^2n}{2R^2} - \frac{A_{55}l^2n}{4R}\right)\sum_{k=1}^{i}C_{i,k}^{(2)} + \left(\frac{A_{55}l^2(n-n^3)}{4R^3}\right)\right\}\bar{\psi}_\theta,$$

$$K_{41} = \left\{+B_{11}\sum_{k=1}^{i}C_{i,k}^{(2)} - B_{55}\frac{n^2}{R^2} + \frac{B_{55}l^2n^2}{4R^2}\sum_{k=1}^{i}C_{i,k}^{(2)} + \left(\frac{5A_{55}l^2n^2}{4R^3} - \frac{B_{55}l^2n^4}{4R^4}\right)\right\}\bar{u},$$

$$K_{42} = -\left\{-\frac{B_{55}n}{R}\sum_{k=1}^{i}C_{i,k}^{(1)} - \frac{B_{12}n}{R}\sum_{k=1}^{i}C_{i,k}^{(1)} - \frac{B_{55}l^2n}{4R}\sum_{k=1}^{i}C_{i,k}^{(3)} - \left(\frac{A_{55}l^2n}{2R^2} + \frac{B_{55}l^2(-n^3+n)}{4R^3}\right)\sum_{k=1}^{i}C_{i,k}^{(1)}\right\}\bar{v},$$

$$K_{43} = -\left\{k_sA_{55}\sum_{k=1}^{i}C_{i,k}^{(1)} - \frac{B_{12}}{R}\sum_{k=1}^{i}C_{i,k}^{(1)} + \frac{A_{55}l^2}{4}\sum_{k=1}^{i}C_{i,k}^{(3)} - \left(\frac{A_{55}l^2(n^2+1)}{4R^2}\right)\sum_{k=1}^{i}C_{i,k}^{(1)}\right\}\bar{w},$$

$$K_{44} = \left\{D_{11}\sum_{k=1}^{i}C_{i,k}^{(2)} - D_{55}\left(\frac{n}{R}\right)^2 - k_sA_{55} + \left(-\frac{D_{55}l^2n^4}{4R^4} + \frac{2B_{55}l^2n^2}{4R^3} - \frac{A_{55}l^2(1+4n^2)}{4R^2}\right) + \left(\frac{D_{55}l^2n^2}{4R^2} + \frac{A_{55}l^2}{4}\right)\sum_{k=1}^{i}C_{i,k}^{(2)}\right\}\bar{\psi}_x,$$

$$K_{45} = \left\{\frac{D_{12}n}{R}\sum_{k=1}^{i}C_{i,k}^{(1)} + D_{55}\frac{n}{R}\sum_{k=1}^{i}C_{i,k}^{(1)} + \frac{D_{55}l^2n}{4R}\sum_{k=1}^{i}C_{i,k}^{(3)} + \left(-\frac{D_{55}l^2n^3}{4R^3} + \frac{B_{55}l^2n}{2R} - \frac{3A_{55}l^2n}{4R}\right)\sum_{k=1}^{i}C_{i,k}^{(1)} - \frac{1}{4R}\frac{\partial A_{55}l^2}{\partial x}(n)\right\}\bar{\psi}_\theta,$$

$$K_{51}=\left\{+\frac{B_{12}n}{R}\sum_{k=1}^{i}C_{i,k}^{(1)}+\frac{B_{55}n}{R}\sum_{k=1}^{i}C_{i,k}^{(1)}+\frac{B_{55}l^2n}{4R}\sum_{k=1}^{i}C_{i,k}^{(3)}-\left(\frac{(B_{55})l^2n}{2R^3}+\frac{A_{55}l^2n}{4R^2}-\frac{B_{55}l^2n^3}{4R^3}\right)\sum_{k=1}^{i}C_{i,k}^{(1)}\right\}\bar{u},$$

$$K_{52}=\left\{B_{55}\sum_{k=1}^{i}C_{i,k}^{(2)}-B_{11}\left(\frac{n}{R}\right)^2+\frac{k_sA_{55}}{R}-\frac{B_{55}l^2}{4}\sum_{k=1}^{i}C_{i,k}^{(4)}-\left(\frac{-3A_{55}l^2}{4R}-\frac{B_{55}l^2}{2R}-\frac{B_{55}l^2(n^2-1)}{4R^2}\right)\sum_{k=1}^{i}C_{i,k}^{(2)}\right.$$
$$\left.+\left(\frac{A_{55}l^2(1-n^2)}{4R^3}\right)+I_1\Omega^2\right\}\bar{v},$$

$$K_{53}=\left\{\frac{k_sA_{55}n}{R}-\frac{B_{11}n}{R^2}+\left(\frac{B_{55}l^2n}{2R^2}-\frac{A_{55}l^2n}{4R}\right)\sum_{k=1}^{i}C_{i,k}^{(2)}+\left(\frac{A_{55}l^2(n-n^3)}{4R^3}\right)\right\}\bar{w},$$

$$K_{54}=-\left\{+\frac{D_{12}n}{R}\sum_{k=1}^{i}C_{i,k}^{(1)}+D_{55}\frac{n}{R}\sum_{k=1}^{i}C_{i,k}^{(1)}+\frac{D_{55}l^2n}{4R}\sum_{k=1}^{i}C_{i,k}^{(3)}+\left(-\frac{D_{55}l^2n^3}{4R^3}+\frac{B_{55}l^2n}{2R}-\frac{3A_{55}l^2n}{4R}\right)\sum_{k=1}^{i}C_{i,k}^{(1)}\right.$$
$$\left.-\frac{1}{4R}\frac{\partial A_{55}l^2}{\partial x}(n)\right\}\bar{\psi}_x,$$

$$K_{55}=\left\{-D_{11}\left(\frac{n}{R}\right)^2+D_{55}\sum_{k=1}^{i}C_{i,k}^{(2)}-k_sA_{55}-\frac{D_{55}l^2}{4}\sum_{k=1}^{i}C_{i,k}^{(4)}+\left(\frac{D_{55}l^2n^2}{4R^2}+\frac{B_{55}l^2}{2R}+A_{55}l^2+\frac{D_{55}l^2}{2R}\right)\sum_{k=1}^{i}C_{i,k}^{(2)}\right.$$
$$\left.+\left(-\frac{A_{55}l^2n^2}{4R^2}-\frac{A_{55}l^2}{4R^2}\right)-\frac{\partial^2D_{55}l^2}{4\partial x^2}\sum_{k=1}^{i}C_{i,k}^{(2)}+I_2\Omega^2\right\}\bar{\psi}_\theta,$$

$$M_{11}=\sum_{i=1}^{N}I_{0i}\bar{u},\qquad M_{14}=\sum_{i=1}^{N}I_{1i}\bar{\psi}_x,\qquad M_{22}=\sum_{i=1}^{N}I_{0i}\bar{v},\qquad M_{25}=\sum_{i=1}^{N}I_{1i}\bar{\psi}_\theta,\qquad M_{33}=\sum_{i=1}^{N}I_{0i}\bar{w},$$

$$M_{41}=\sum_{i=1}^{N}I_{1i}\bar{u},\qquad M_{44}=\sum_{i=1}^{N}I_{2i}\bar{\psi}_x,\qquad M_{52}=\sum_{i=1}^{N}I_{1i}\bar{v},\qquad M_{55}=\sum_{i=1}^{N}I_{2i}\bar{\psi}_\theta,$$

$$M_{12}=M_{13}=M_{15}=M_{21}=M_{23}=M_{24}=M_{31}=M_{32}=M_{34}=M_{35}=M_{42}=M_{43}=M_{45}=M_{51}=M_{53}=M_{54}=0,$$

$$\mathrm{C}_{23}=-2\sum_{i=1}^{N}I_{0i}\Omega_i,\qquad \mathrm{C}_{32}=2\sum_{i=1}^{N}I_{0i}\Omega_i,\qquad \mathrm{C}_{35}=2\sum_{i=1}^{N}I_{1i}\Omega_i,\qquad \mathrm{C}_{53}=-2\sum_{i=1}^{N}I_{1i}\Omega_i,$$

$$\mathrm{C}_{11}=\mathrm{C}_{12}=\mathrm{C}_{13}=\mathrm{C}_{14}=\mathrm{C}_{15}=\mathrm{C}_{21}=\mathrm{C}_{22}=\mathrm{C}_{24}=\mathrm{C}_{25}=\mathrm{C}_{31}=\mathrm{C}_{33}=\mathrm{C}_{34}=\mathrm{C}_{41}=\mathrm{C}_{42}=\mathrm{C}_{43}=\mathrm{C}_{44}=\mathrm{C}_{45}$$
$$=\mathrm{C}_{51}=\mathrm{C}_{52}=\mathrm{C}_{54}=\mathrm{C}_{55}=0.$$

References

1. M. Eftekhari, S. Mohammadi, A.R. Khoei, Comput. Mater. Sci. **79**, 736 (2013).
2. I. Elishakoff, D. Pentaras, J. Sound Vib. **322**, 652 (2009).
3. M. Zidour, K.H. Benrahou, A. Semmah, M. Naceri, H.A. Belhadj, K. Bakhti *et al.*, Comput. Mater. Sci. **51**, 252 (2012).
4. J. Yoon, C. Ru, A. Mioduchowski, Compos. Sci. Technol. **65**, 1326 (2005).
5. C. Rao, A. Cheetham, J. Mater. Chem. **11**, 2887 (2001).
6. C. Li, L. Chen, J. Shen, J. Mech. **31**, 7 (2015).
7. G. Hummer, J.C. Rasaiah, J.P. Noworyta, Nature **414**, 188 (2001).
8. Z. Yang, M. Nakajima, Y. Shen, T. Fukuda, *Nano-gyroscope assembly using carbon nanotube based on nanorobotic manipulation*, in *2011 International Symposium on Micro-NanoMechatronics and Human Science (MHS)* (IEEE, 2011) pp. 309–314 DOI: 10.1109/MHS.2011.6102199.
9. Q. Tu, Q. Yang, H. Wang, S. Li, Sci. Rep. **6**, 26183 (2016).
10. M. Ghadiri, N. Shafiei, H. Safarpour, Microsyst. Technol. (2016) DOI: 10.1007/s00542-016-2822-6.
11. M. Ghadiri, H. SafarPour, J. Therm. Stresses (2016) DOI: 10.1007/s00542-016-2822-6.
12. R.A. Toupin, Arch. Ration. Mech. Anal. **11**, 385 (1962).
13. W. KoLter, Proc. K. Nederl. Akaad. van Wetensch **67**, 17 (1964).
14. R.D. Mindlin, Arch. Ration. Mech. Anal. **16**, 51 (1964).
15. M. Asghari, M. Kahrobaiyan, M. Rahaeifard, M. Ahmadian, Arch. Appl. Mech. **81**, 863 (2011).
16. F. Yang, A. Chong, D. Lam, P. Tong, Int. J. Solids Struct. **39**, 2731 (2002).
17. S. Park, X. Gao, J. Micromech. Microeng. **16**, 2355 (2006).

18. J. Reddy, J. Mech. Phys. Solids **59**, 2382 (2011).
19. M. Shaat, F. Mahmoud, X.-L. Gao, A.F. Faheem, Int. J. Mech. Sci. **79**, 31 (2014).
20. E.M. Miandoab, H.N. Pishkenari, A. Yousefi-Koma, H. Hoorzad, Physica E **63**, 223 (2014).
21. E. Reissner, J. Appl. Mech. **12**, 69 (1945).
22. R.D. Mindlin, J. Appl. Mech. **18**, 31 (1951).
23. M. Torkaman-Asadi, M. Rahmanian, R. Firouz-Abadi, Compos. Struct. **126**, 52 (2015).
24. G.H. Bryan, *On the beats in the vibrations of a revolving cylinder or bell*, in *Proceedings of the Cambridge Philosophical Society* (1890) pp. 101–111.
25. R. DiTaranto, M. Lessen, J. Appl. Mech. **31**, 700 (1964).
26. A. Zohar, J. Aboudi, Int. J. Mech. Sci. **15**, 269 (1973).
27. J. Padovan, J. Sound Vib. **31**, 469 (1973).
28. J. Padovan, Int. J. Solids Struct. **11**, 1367 (1975).
29. J. Padovan, Comput. Struct. **5**, 145 (1975).
30. M. Endo, K. Hatamura, M. Sakata, O. Taniguchi, J. Sound Vib. **92**, 261 (1984).
31. T. Saito, M. Endo, J. Sound Vib. **107**, 17 (1986).
32. S. Huang, W. Soedel, J. Appl. Mech. **55**, 231 (1988).
33. S. Huang, B. Hsu, J. Sound Vib. **136**, 215 (1990).
34. T.R. Tauchert, *Energy principles in structural mechanics* (McGraw-Hill Companies, 1974).
35. S. Hosseini-Hashemi, M. Ilkhani, M. Fadaee, Int. J. Mech. Sci. **76**, 9 (2013).
36. R. Bellman, J. Casti, J. Math. Anal. Appl. **34**, 235 (1971).
37. R. Bellman, B. Kashef, J. Casti, J. Comput. Phys. **10**, 40 (1972).
38. F. Tornabene, N. Fantuzzi, M. Bacciocchi, *The strong formulation finite element method: stability and accuracy*, in *Frattura ed Integrità Strutturale* (2014) p. 251.
39. F. Tornabene, N. Fantuzzi, F. Ubertini, E. Viola, Appl. Mech. Rev. **67**, 020801 (2015).
40. C. Shu, *Differential Quadrature and its Application in Engineering* (Springer Science & Business Media, 2012).
41. C. Shu, B.E. Richards, Int. J. Numer. Methods Fluids **15**, 791 (1992).
42. Ö. Civalek, Eng. Struct. **26**, 171 (2004).
43. M. Ghadiri, H. Safarpour, Appl. Phys. A **122**, 833 (2016).
44. Y.T. Beni, F. Mehralian, H. Razavi, Compos. Struct. **120**, 65 (2015).
45. A. Alibeigloo, M. Shaban, Acta Mech. **224**, 1415 (2013).
46. Y. Tadi Beni, F. Mehralian, H. Zeighampour, Mech. Adv. Mater. Struct. **23**, 791 (2016).